

Review

# Electrochemical Perovskite-Based Sensors for the Detection of Relevant Biomarkers for Human Kidney Health

Claudia Ivone Piñón-Balderrama <sup>1,\*</sup>, César Leyva-Porras <sup>1</sup>, Alain Salvador Conejo-Dávila <sup>2</sup>, Anayansi Estrada-Monje <sup>2</sup>, María Cristina Maldonado-Orozco <sup>3</sup>, Simón Yobanny Reyes-López <sup>4</sup>, and Erasto Armando Zaragoza-Contreras <sup>1,\*</sup>

- <sup>1</sup> Centro de Investigación en Materiales Avanzados, S.C., Miguel de Cervantes No. 120, Complejo Industrial Chihuahua, Chihuahua C.P. 31136, Chihuahua, Mexico; cesar.leyva@cimav.edu.mx
- <sup>2</sup> Centro de Innovación Aplicada en Tecnologías Competitivas, Omega No. 201 Col. Industrial Delta, León C.P. 37545, Guanajuato, Mexico; alain.conejo@cimav.edu.mx (A.S.C.-D.); aestrada@ciatec.mx (A.E.-M.)
- <sup>3</sup> Faculty of Engineering, Universidad Autónoma de Chihuahua, Circuito Número 1 s/n, Nuevo Campus Universitario, Nte. 2, Chihuahua C.P. 31125, Chihuahua, Mexico; cmaldona@uach.mx
- <sup>4</sup> Institute of Biomedical Sciences, Universidad Autónoma de Ciudad Juárez, Envolverte del PRONAF and Estocolmo s/n, Ciudad Juárez C.P. 32310, Chihuahua, Mexico; simon.reyes@uacj.mx
- \* Correspondence: claudia.pinion@cimav.edu.mx (C.I.P.-B.); armando.zaragoza@cimav.edu.mx (E.A.Z.-C.)

**Abstract:** The importance of biomarker quantification in technology cannot be overstated. It has numerous applications in medical diagnostics, drug delivery, and the timely implementation of prevention and control strategies for highly prevalent diseases worldwide. However, the discovery of new tools for detection has become increasingly necessary. One promising avenue is the use of perovskite-based materials, which exhibit excellent catalytic activity and redox properties. These make them ideal candidates for the development of electrochemical sensors. In this review, the advances of purely non-enzymatic electrochemical detection of bio-analytes, with ABO<sub>3</sub> perovskite form, are presented. The work allows the visualization of some of the modifications in the composition and crystal lattice of the perovskites and some variations in the assembly of the electrodes, which can result in systems with a better response to the detection of analytes of interest. These findings have significant implications for improving the accuracy and speed of biomarker detection, ultimately benefiting patients and healthcare professionals alike.

**Keywords:** non-enzymatic; electrochemical; perovskite-based sensor; human health biomarkers; glucose; hydrogen peroxide; urea; uric acid



**Citation:** Piñón-Balderrama, C.I.; Leyva-Porras, C.; Conejo-Dávila, A.S.; Estrada-Monje, A.; Maldonado-Orozco, M.C.; Reyes-López, S.Y.; Zaragoza-Contreras, E.A. Electrochemical Perovskite-Based Sensors for the Detection of Relevant Biomarkers for Human Kidney Health. *Chemosensors* **2023**, *11*, 507. <https://doi.org/10.3390/chemosensors11090507>

Academic Editor: Núria Serrano

Received: 1 August 2023

Revised: 11 September 2023

Accepted: 15 September 2023

Published: 17 September 2023



**Copyright:** © 2023 by the authors. Licensee MDPI, Basel, Switzerland. This article is an open access article distributed under the terms and conditions of the Creative Commons Attribution (CC BY) license (<https://creativecommons.org/licenses/by/4.0/>).

## 1. Introduction

Non-protein nitrogenous compounds (NPNC) such as urea, uric acid, creatine, and creatinine are commonly used as biomarkers of human kidney health. Worldwide acute kidney injury (AKI) in critically ill patients is a risk factor for morbidity and mortality, with a prevalence of 17.2% in the short and long term, representing important economic impacts in terms of public health costs with an estimated USD 10 billion [1]. In 2005, the American Society of Nephrology Renal Research Report (ASNRRR) assigned the highest research priority for the discovery, detection, and standardization of novel AKI biomarkers [2]. Hydrogen peroxide and glucose are also recognized as critical biomarkers of renal function in patients with chronic kidney disease, which can lead to progressive loss of organ function and eventually to end-stage renal disease [3,4]. A biomarker is defined as a molecular marker that indicates a biological state. Biomarkers are substances in the blood, tissues, and other biological fluids, such as urine or saliva, the presence and level of which indicate a normal or abnormal condition or disease. Currently, there is great scientific and commercial interest in the discovery of new biomarkers and the development of novel techniques for their detection and quantification. As known, once a biomarker is associated

with a disease, the chances and efficacy of the treatments are more successful, while the corresponding commercial opportunities for biotechnology and pharmaceutical companies are triggered. A biomarker can be a gene, a protein, a metabolite, or a substance that can be studied qualitatively and quantitatively by analytical methods such as colorimetric [5], spectrophotometric [6], and chromatographic [7] methods. Although these methods have the advantage of being highly sensitive and selective for many biomarkers, their detection is slow and expensive, and samples require pretreatment and use highly specialized material and equipment, which makes diagnosis a late and expensive event. Commonly, these types of methods are found in hospitals and specialized clinics. The emergence of new tools for the quantification of health biomarkers can potentially improve this situation, allowing the early use of multiple treatment strategies for the preservation of human health and promoting the commercial availability of at-home detection devices. Currently, some sensor systems and biosensors are emerging as promising alternatives, overcoming the drawbacks. Such devices combine biological recognition elements through a transducer responsible for giving a signal response to the presence of the biomarker and converting the observed change into a measurable signal. Diverse elements of biological recognition have been explored in numerous studies, such as biocatalysts (enzymes, microorganisms, material tissue) and bioligands (antibodies, nucleic acids, and lipid layers) [8,9]. The usefulness of these systems is impressive; however, their complexity and dependence on multiple components present the disadvantages of low storage stability, probability of enzyme inactivation, high cost, and complexity of operation. In addition, variations in sensor activity may be introduced by factors such as pH, the presence of inhibitory agents, and enzyme immobilization [10–12].

In recent decades, novel sensors have been developed for the detection of various biomarkers, primarily for those with a response that can be detected by colorimetric [5,13], fluorescent [14], or electrochemical [15] methods. This type of sensor has attracted attention due to its relative ease in the development of commercial devices, and at the same time, it has the advantage of not being invasive; i.e., the patient is spared the trauma of taking a blood sample since it is acquired from other bodily fluids such as saliva, sweat, urine, or tears [16–19]. These non-invasive sensors are based on electrodes, where the electrocatalytic oxidation of analytes is carried out on the surface. Therefore, the selection of the electrode and its surface characteristics, like morphology, porosity, rugosity, composition, and electron transport, significantly impact the final performance of the sensor [20].

Perovskite-based electrodes were first reported by Shimizu et al. in 1996 [21]. Since then, perovskites have shown great potential for easy-to-use detection device development with outstanding performance in detecting a variety of chemical and biological species. Either in the solid state or in solution, perovskites exhibit high selectivity and sensitivity, while providing stability to sensors. The performance of the perovskite-based sensors is due to the tunable redox properties, high oxygen mobility, electronic and ionic conduction, thermal and chemical stability, oxygen sorption capacity, and active electrical structure; all these features make this material an attractive support for the efficient detection of important biomarkers [22–24].

In this review, we report the recent advances in non-enzymatic electrochemical perovskite-based sensors focused on three types of biomarkers related to relevant aspects of human health for renal health indicators: glucose, hydrogen peroxide, and NPNC such as urea. This review also includes the use of perovskites with different cations, partial substitution, and different dopants, aiming to identify those that have demonstrated a better performance for the detection of the biomarkers of interest in electrochemical sensors.

## 2. Perovskite's Overview

Perovskites are materials with a chemical formula of the form  $ABO_3$  (oxide-based form) or  $ABX_3$  (halogen-based form), ordered in a specific arrangement of atoms in a crystal lattice. It consists of a cubic unit cell in which an atom or ion is located at the center, surrounded by a larger octahedral cage of different atoms or ions. In the structure, A and B

represent cations of different sizes (Figure 1A). In the crystalline structure of perovskites, cations in position A are usually the larger cations corresponding to alkali, alkaline earth, or lanthanide elements. These cations form a cubic lattice, which occupies the body center, 12-coordinate position. Cations B are mostly medium-sized transition metals with a preference for octahedral coordination with oxygen atoms [25,26]. Adsorption and porosity have been identified as key parameters for the sensing ability of perovskite electrochemical sensors. Thus, many works have been dedicated to evaluating the relationship between synthesis processes and morphology [27–30]. The overall conclusion is that to improve the sensing performance, the surface area must be increased, the grain size reduced, and a porous structure created. For example, Wang et al. [31] prepared  $\text{LaNiO}_3$  perovskites by electrospinning, decreasing the diameter from 400 to 140 nm by removing the binding agent (polyvinyl pyrrolidone) through calcination. With this, the surface of the fibers became rough, increasing the specific surface area and the number of active sites for the electrochemical reaction. The variation of dopants A and B and the partial substitution of B positions with cations of similar redox behavior (B') is another strategy employed to improve the redox efficiency of perovskites.  $\text{LaMnO}_3$  perovskites and their corresponding B partial substitution  $\text{La}_{1-x}\text{A}_x\text{Mn}_{1-y}\text{M}_y\text{O}_3$  (where M is a transition metal like Fe, Co, or Ni) showed possibilities to improve the sensing capacity of the hydrogen peroxide due to different oxidation states of the metal, Mn(II), Mn(III), and Mn(IV), and a flexible oxygen stoichiometry [32]. Other studies have focused on how the modification of cations induces distortion of the original form of the  $\text{ABO}_3$  formula and its effects on the perovskite catalytic properties [33–36]. The modification of the general formula induces changes in the symmetry of the crystalline structure and hence distortions in the original monoclinic, orthogonal, tetragonal, or cubic phases [37]. Although the literature mainly attributes the electrocatalytic properties to cation B, which participates in the redox process of several analytes, the ultra-high catalytic activity of perovskites seems to be due to a synergistic effect of A and B dopants since cation A also promotes the electrocatalytic activity by inducing a high concentration of non-stoichiometric oxygen (oxygen vacancies), a high diffusion rate of oxygen ions, an increase in the charge transfer process, and a stabilization of different oxidation states of B cations [38–41].

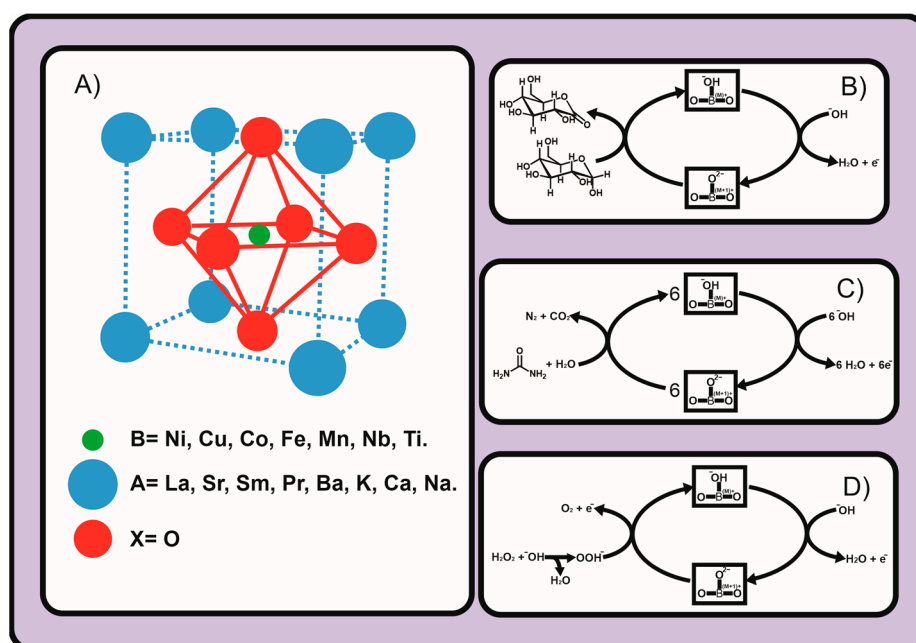


**Figure 1.** (A) Schematic representation of  $\text{ABO}_3$  perovskite structure. Redox mechanism of (B) glucose, (C) urea, and (D) hydrogen peroxide.

The detection mechanism in non-enzymatic electrochemical detection of bioanalytes with  $ABO_3$  perovskites is based on the chemical reaction of B cations with OH groups in an alkaline medium, forming oxides, hydrated oxides, or hydroxide species (Figure 1B). He et al. [42] reviewed the advances in non-enzymatic electrochemical sensing using oxidized perovskites. In this review, the model of the incipient hydrated oxide adatom mediator (IHOAM) was introduced, which is the model that better describes the mechanism of electrochemical sensing. According to this model, the metals oxidize at a low potential and produce hydrated oxides (BOOH) that mediate oxidation and reduction processes [43]. A particular emphasis was placed on the effect of the electrocatalytic mechanism of lattice oxygen intermediates (LOM) with adsorbed -OO and lattice O vacancies [44], which endow these perovskites with ultra-high catalytic activity. Several other review papers have been focused on the perovskites' sensory applications based on their ferroelectric, ferromagnetic, optical, and electrical properties [45–48].

### 3. Application of Perovskites in the Sensing of NPNC Biomarkers

#### 3.1. Sensing of Glucose

Glucose, as the major energy supply substance of organisms and an intermediate product of metabolism, plays a vital role in the physiology and biochemistry of living organisms. Glucose promotes the body's ability to remember, stimulates calcium absorption, and increases cellular communication [49]. However, the overexpression of serum glucose triggers adverse effects in the body, leading to chronic damage and dysfunction of various tissues, especially diabetic retinopathy, diabetic cataracts, and peripheral neuropathy. Hence, there is value in detecting and quantifying the glucose content in the human body. Traditional home blood glucose monitoring (HBGM) methods are invasive, involving blood analysis through a blood drop from one fingertip, the reaction of the glucose in the blood with the indicator band, and the final reading content on the glucometer screen. This type of biosensor is based on a thin layer of glucose oxidase (GOx) on an oxygen electrode. Thus, the readout is the amount of oxygen consumed by GOx during the enzymatic reaction with the substrate glucose [50]. In the test strip, a GOx enzyme reacts with glucose to create gluconic acid. The gluconic acid reacts with ferricyanide, which then combines to create ferrocyanide. The amount of ferrocyanide produced is related to the glucose concentration in the blood sample by an electronic current passing through the testing strip. The glucose concentration is indicated by the number displayed on the screen of the glucose testing meter. A comprehensive review of electrochemical glucose biosensors was reported by Wang [51]. According to this review, glucose biosensors can be categorized into three groups: (i) first-generation biosensors that require the use of a natural oxygen co-substrate, the generation and detection of hydrogen peroxide ( $H_2O_2$ ), and the application of a relatively high potential on the electrode; (ii) second-generation biosensors that involve replacing the oxygen co-substrate with a synthetic electron acceptor capable of transporting electrons from the enzyme to the surface of the electrode; and (iii) third-generation biosensors that are based on the elimination of the electron-transfer mediator and the application of a relatively low operating potential.

Recently, the development of non-enzymatic glucose biosensors has been directed toward the obtention of non-invasive detection mechanisms, which avoids the hassle of taking a blood sample through determinations in other body biological fluids such as saliva, sweat, urine, and tears. The study of non-enzymatic sensors also has given rise to detection systems with reduced costs, avoiding the use of expensive and unstable enzymes. The use of enzymes presents the disadvantage of low stability, in addition to variations in sensory activity due to factors such as pH, the presence of inhibitory agents, and enzyme immobilization [12,52,53]. These non-invasive sensors are based on electrodes where the electrocatalytic oxidation of analytes is carried out on the surface. Therefore, the selection of the material for modifying the electrode surface, the electroactive area, morphology, porosity, and rugosity can significantly impact the final performance of the sensor [20].  $NiFe_2O_4$  (NFO) nanoparticles were used to immobilize GOx on a carbon paste electrode

(CPE) coated with  $\text{LaNi}_{0.5}\text{Ti}_{0.5}\text{O}_3$  (LNT) perovskite particles, finding that at a ratio of 20:1 LNT-NFO, the enzymes were effectively immobilized, obtaining a glucose sensor with a linear range of 0.5–10 mM and a detection limit of 0.04 mM [54]. In this sense, perovskites are materials able to retain a three-dimensional network microstructure while keeping large amounts of oxygen vacancies and accommodating different metallic elements within the lattice structure [55]. A recent review established that the mechanism for glucose electro-oxidation in perovskites is complex and similar to the mechanism of  $\text{H}_2\text{O}_2$  electro-oxidation [56]. This mechanism is known as the lattice-oxygen-mediated oxygen evolution reaction (LOM-OER), which involves the partial substitution of the cations of the A sites by divalent cations from group IIA of the periodic table, which can oxidize the cations of the B sites. The increase in these substitutions causes a reduction in the formation energy of oxygen vacancies, which transfer oxygen from the lattice to the adsorbed species, generating highly oxidative oxygen species known as superoxide ions.

The first published article where perovskites were employed as a sensor on a carbon electrode in electrochemical tests was published by Shimizu et al. in 1996 [21]. They found that  $\text{La}_{0.6}\text{Ca}_{0.4}\text{Ni}_{0.7}\text{Fe}_{0.3}\text{O}_3$  perovskite presented a relatively high specific surface area and good response in the sensing of  $\text{H}_2\text{O}_2$  in the range of 0.01–1 mM. In the  $\text{A}_2\text{BO}_{4+\delta}$  type perovskite containing  $\text{Pr}_{1.92}\text{Ba}_{0.08}\text{Ni}_{0.95}\text{Zr}_{0.05}\text{O}_{4+\delta}$ , the presence of  $\text{Pr}_2\text{O}_3$  promotes the formation of defects in the crystal lattice of the A sites, as the partial substitution of Pr by Ba causes the disproportionation (oxidation-reduction reaction) of the B sites from  $\text{Ni}^{\text{III}}$  to  $\text{Ni}^{\text{II}}$  and  $\text{Ni}^{\text{IV}}$  [56]. The perovskite material was deposited on a gold electrode employed as a working electrode, and the performance of the glucose sensor showed a dynamic range of 1.5–7000  $\mu\text{M}$ , detection limit of 0.5  $\mu\text{M}$ , and no interference for glucose detection in human serum.

The properties of the perovskites are mainly determined by the element, substitution, and occupation of the B sites [57]. In this sense, perovskites doped with noble metals ( $\text{AB}_{1-y}\text{M}_y\text{O}_3$ ) may present improved stability and catalytic activity. To verify this, the  $\text{SrPd}_{1-y}\text{M}_y\text{O}_3$  perovskites were studied, where M represents the noble metals tested ( $\text{Ni}^{2+}$ ,  $\text{Cu}^{2+}$ ,  $\text{Au}^{3+}$ , and  $\text{Pt}^{2+}$ ) [58]. From these cations,  $\text{Au}^{3+}$  at low concentrations, i.e.,  $0 < y < 0.7$ , presented the best characteristics for glucose sensing since the anodic peak current increased, reaching a maximum value at  $y = 0.3$ . The dopant promoted the electronic properties of the perovskite and increased the charge transfer rate while stabilizing the orthorhombic structure. The glucose sensing in human serum showed a wide concentration range of 0.2–1000  $\mu\text{M}$ , high sensitivity of  $1.44 \times 10^4 \mu\text{A}/\text{mM cm}^2$ , low detection limit of 2.11 nM, and no interference from other molecules. Silver nanoparticles have been extensively studied as catalysts in various reactions due to their excellent electrical conductivity. Hence, by adding Ag NPs to a La-Ti perovskite ( $\text{LaTiO}_3\text{-Ag}0.2$ ), it has been possible to decrease the detection limit to 0.21  $\mu\text{M}$ , increase the sensitivity to  $784.14 \mu\text{A}/\text{mM cm}^2$ , and broaden the range of linear response of 2.5  $\mu\text{M}$  to 4 mM [59].

Perovskites containing Ni at the B sites, known as nickelates ( $\text{ANiO}_3$ , where A = La, Nd, Eu, Gd, Dy, or Sm), have also attracted the attention of glucose sensing due to their specific conductivity, specific surface area, and electroactivity. The contribution of some of these rare earths in the A position of the perovskite, as in the case of Nd, is to provide a high specific conductivity to the electrode. For example,  $\text{NdNiO}_3$  perovskite synthesized by the hydrothermal method and deposited on a carbon electrode showed excellent electrocatalytic behavior for the oxidation of glucose in human serum [60]. The electrochemical results showed a wide linear range from 0.5  $\mu\text{M}$  to 4.6 mM, a sensitivity of  $1105.1 \mu\text{A}/\text{mM cm}^2$ , and a detection limit of 0.3  $\mu\text{M}$ . The non-enzymatic glucose oxidation mechanism in this type of perovskite involves the oxidation of nickel ( $\text{Ni}^{2+} \leftrightarrow \text{Ni}^{3+} + \bar{e}$ ) and the subsequent oxidation of glucose ( $\text{Ni}^{3+} + \text{glucose} \rightarrow \text{Ni}^{2+} + \text{glucolactone}$ ).  $\text{LaNi}_{0.5}\text{Ti}_{0.5}\text{O}_3$  (LNT) deposited on a carbon paste electrode (CPE) showed a sensitivity to glucose of  $1630.53 \mu\text{A}/\text{mM cm}^2$ , limit of detection of 0.07  $\mu\text{M}$ , and linear range of 0.2 to 20  $\mu\text{M}$  [61]. In electrodes modified with perovskites of  $\text{La}_{0.6}\text{Sr}_{0.4}\text{FeO}_{3-\delta}$  and  $\text{La}_{0.6}\text{Sr}_{0.4}\text{Co}_{0.2}\text{Fe}_{0.8}\text{O}_{3-\delta}$  (LSF and LSCF, respectively), the partial substitution of Fe by Co atoms increased the sensitivity towards the detection of  $\text{H}_2\text{O}_2$  and glucose [62]. The partially occupied *d* orbitals allow these transition metals to

assume different oxidation states through the loss or acquisition of electrons, which promote the formation of a surface layer of adsorbed OH species. Glucose detection results for the LSCF perovskite obtained at a potential of 0.5 V were a linear range of 0–200  $\mu\text{M}$ , detection limit of 7  $\mu\text{M}$ , and sensitivity of 285  $\mu\text{A}/\text{mM cm}^2$ .

The formation of oxygen vacancies has also been identified as a key parameter to increase the glucose sensing capacity through surface area modification. He et al. studied the increase of oxygen vacancies by replacing trivalent cations such as  $\text{La}^{3+}$  with divalent cations such as  $\text{Sr}^{2+}$  or  $\text{Ca}^{2+}$ . Additionally, the presence of these cations promotes a growth in surface area and structural stability. The doping of the  $\text{SrPO}_3$  perovskite with Ca, in the concentration range of 0–0.7, allowed setting the formulation  $\text{Sr}_{1.7}\text{Ca}_{0.3}\text{PdO}_3$  with optimal results in glucose sensing [63]. This performance was mainly attributed to the structural modification of the crystalline lattice, where the increase in the free volume allows a greater mobility of the surface lattice oxygen. The sensing results showed a linear range of 5  $\mu\text{M}$  to 1.4 mM, a sensitivity of 306.9  $\mu\text{A}/\text{mM cm}^2$ , and a detection limit of 0.0845  $\mu\text{M}$ . Determining glucose in urine samples showed relative standard deviations lower than 4.17%. In the case of the perovskite  $\text{La}_{0.6}\text{Sr}_{0.4}\text{CoO}_{3-\delta}$  (LSC), its behavior as a glucose sensor was enhanced by depositing on a reduced graphite oxide (RGO) electrode, presenting a detection range of 2–3350  $\mu\text{M}$ , sensitivity of 330  $\mu\text{A}/\text{mM cm}^2$ , and detection limit of 0.063  $\mu\text{M}$  [64].

Surface area and grain size modification and the creation of porous structures represent an alternative strategy to improve the sensing performance of perovskite-based materials. For example,  $\text{LaNiO}_3$  perovskites, prepared by electrospinning, showed a decrease in the diameter of the fibers after the removal of polyvinyl pyrrolidone by calcination, which worked as the binding agent. The reduction of the fibers decreased from 400 to 140 nm, giving rise to a rougher surface and increasing the specific surface area and the number of active sites for the electrochemical reaction. The Ni ions are the active sites with partially occupied  $d$  orbitals that produce two different oxidation states for the metal ( $\text{Ni}^{\text{II}}/\text{Ni}^{\text{III}}$ ). The detection limit for glucose was 0.32  $\mu\text{M}$  and a linear detection range of up to 1 mM. Electrospun and calcined  $\text{La}_{0.88}\text{Sr}_{0.12}\text{MnO}_3$  perovskites deposited on a CPE presented a linear range of 0.05–100  $\mu\text{M}$ , a sensitivity of 1111  $\mu\text{A}/\text{mM cm}^2$ , and a detection limit of 32 nM [31]. The morphological characterization showed rough surface fibers with diameters of 200–300 nm and lengths of several micrometers.  $\text{ABO}_3$ -type perovskite structures were employed for modifying a carbon electrode with the electrospinning of porous La–Sr–Co–Ni–O (LSCNO) nanofibers [65]. According to these authors, when metallic elements such as Ni, Co, and Fe are placed in perovskite B sites, they promote a high activity in glucose sensing. Then, after testing the perovskite's performance in glucose detection, they found an optimal composition of the form  $\text{La}_{0.75}\text{Sr}_{0.25}\text{Co}_{0.5}\text{Ni}_{0.5}\text{O}_3$ , showing a linear response in the range of 0.1–1.0 mM with a calibration sensitivity of  $924 \pm 28 \mu\text{A}/\text{mM}$ , a low detection limit of 0.083 mM, and  $0.59 \pm 0.03$  mM of glucose in urine fluid sample.

Because of its high electrocatalytic activity, perovskite-carbon nitride composite is an attractive potential candidate for interference-free sensing of glucose [66]. A perovskite-type cerium-aluminum oxide ( $\text{CeAlO}_3$ , molar ratio Ce: Al of 1:1), in the form of polycrystalline powder, was ultrasonically mixed with carbon nitride (CN). The formed  $\text{CeAlO}_3@\text{CN}$  composite was deposited on a glassy carbon electrode, represented in Figure 2. Then, it was tested as the working electrode in a conventional electrochemical three-electrode cell configuration. The voltammetry detection of glucose showed a linear concentration range of 0.01–1034.5  $\mu\text{M}$  and a detection limit of 0.86 nM. The amperometric determinations of glucose in human blood, saliva, and sweat were compared against those determined in a commercial glucometer, finding similar results with less than five percent error. A photoelectrochemical biosensor based on different semiconductor heterojunctions was constructed to reduce electron–hole pair recombination while retaining the oxidation potential of the composite material [67]. For this purpose, strontium titanate ( $\text{SrTiO}_3$ ) perovskite was synthesized by hydrothermal method and employed as a working electrode in tandem with titanium oxide ( $\text{TiO}_2$ ), polydopamine (PDA), and GOx. PDA was deposited on the final surface of the modified electrode and employed as the binder to increase the

affinity between GOx and the perovskite. The  $\text{TiO}_2\text{-SrTiO}_3\text{-PDA-GOx}$  system presented an extended linear range of 0–32 mM, a high sensitivity of  $5.37 \mu\text{A}/\text{mM cm}^2$ , a detection limit of  $25.68 \mu\text{M}$ , and accurate detection of glucose in human serum in the range of 0–20 mM. The proposed mechanism describes hydrogen peroxide production from the surface reaction of glucose and GOx and its subsequent oxidation by photogenerated holes at the  $\text{SrTiO}_3\text{-TiO}_2$  interface to generate a photocurrent. The  $\text{SrPdO}_3$  perovskite coated with gold nanoparticles presented a synergistic effect with a higher current response for the electro-detection of glucose with a linear concentration range of  $100 \mu\text{M}/\text{L}$  to  $6 \text{mM}/\text{L}$ , detection limit of  $10 \mu\text{M}/\text{L}$ , and no interferences detection [63]. This system allowed the glucose oxidation mechanism explanation based on the oxidation potentials: (i) the dehydrogenation of the adsorbed glucose molecules ( $-0.55 \text{V}$ ), (ii) oxidation of dehydrogenated glucose ( $+0.056 \text{V}$ ) to gluconolactone, and (iii) conversion of gluconolactone to gluconate by reacting with hydroxyl ions in solution.

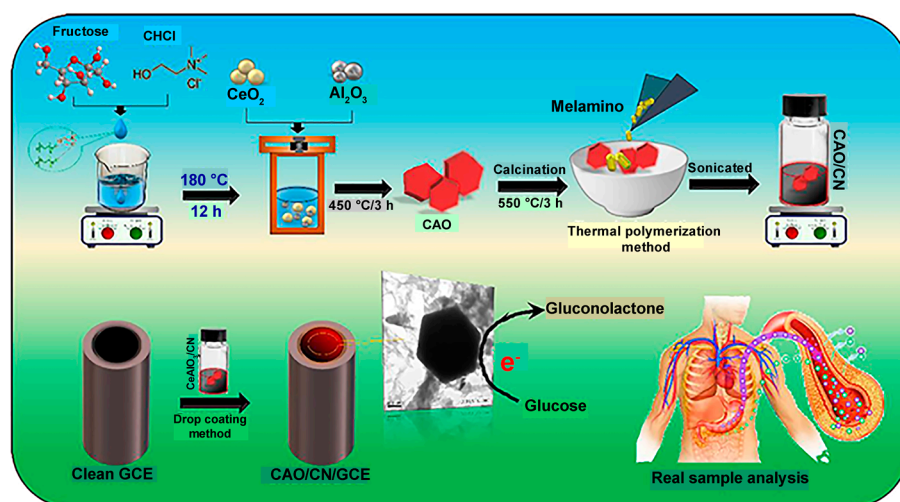


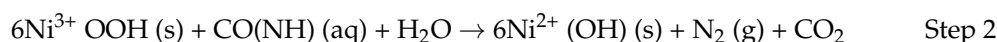
**Figure 2.** Schematic representation of the electrochemical detection of glucose sensing. Reprinted from publication. Deep eutectic solvents synthesis of perovskite-type cerium aluminate embedded carbon nitride catalyst: High-sensitive amperometric platform for sensing of glucose in biological fluids. 102, 312–320. Rajaji et al. Copyright (2021) with permission from Elsevier [66].

Other glucose sensing techniques not based on electrochemical measurements include colorimetry, fluorometry, and chemiluminescence. The hydrolysis reaction of glucose by GOx produces water, oxygen, and many protons, lowering the pH and harshening the environment of the sensing probe. Thus, cesium-lead-bromide perovskite quantum dots were coated with  $\text{SiO}_2$  ( $\text{CsPbBr}_3@ \text{SiO}_2$  PQDs) to avoid environmental deterioration and the loss of optical properties such as light emission. This system showed excellent fluorescence properties with an absorption of UV radiation at a wavelength of 365 nm, an emission of green light at 525 nm, a notable selectivity to pH, and a detection limit of  $18.5 \mu\text{M}$  [68]. The development of fluorescence measurements by eliminating multiple background interferences has led to a noticeable improvement in detection sensitivity and accuracy. This has been achieved by exciting a material at one wavelength and obtaining emission at two wavelengths. Metal halide perovskite nanocrystals present unique optical properties for this purpose.  $\text{CsPbBr}_3$  hydride perovskite nanocrystals (PNCs) complexed with Cu NCs emit at two wavelengths: PNCs at 645 nm and NCs at 517 nm [69]. Upon the glucose sensing, the system presented a linear response range of  $2.0\text{--}170.0 \mu\text{M}$ , a detection limit of  $0.8 \mu\text{M}$ , and satisfactory results when tested with human serum. Electrochemiluminescence (ECL) sensors are based on the synergistic effect of electrochemical oxidation or reduction of a chemical compound that emits light. With  $\text{LaTiO}_3\text{-Ag}_{0.1}$  deposited on a working electrode and luminol as a chemiluminescent agent, a promising glucose sensor was reported [70]. Properties as glucose sensors in human blood serum samples have a linear range of  $0.01 \mu\text{M}$ –

0.10 mM, a detection limit of 2.50 nM, and a sensitivity of  $7.80 \times 10^2 \mu\text{A}/\text{mM cm}^2$ . These properties are explained in terms of the increase of the active surface area of the working electrode caused by the perovskite composite oxide, while doping with Ag promotes the interfacial electron-transfer rate, and the luminol oxidation generates the ECL effect.

### 3.2. Sensing of Urea

According to the definition of the British encyclopedia [71], urea is a nitrogenous product of the metabolic breakdown of proteins in all mammal species, present in the urine, blood, bile, milk, and all mammal species perspiration. While the proteins break down, amino groups are removed from the amino acids, which could convert later to ammonia, which is toxic to the body and converted into urea by the liver. The urea then passes to the kidneys and is excreted in the urine. If this process is disturbed, ammonia levels begin to rise. High urea levels in blood and urine cause kidney failure, urinary tract obstruction, gastrointestinal bleeding, dehydration, burns, and shock, while lower levels of urea result in hepatic failure, nephritic syndrome, and cachexia [72–74]. The electrochemical oxidation of urea from perovskite-based sensors is catalyzed by cation B. In an alkaline medium, the adsorption of  $\text{OH}^-$  groups takes place on the electrode surface. Then, these groups react with the B metal to form the  $\text{M}^{2+}(\text{OH})_2$  species. These molecules are oxidated to produce  $\text{M}^{3+}\text{OOH}$ , corresponding to the reactive species that carry out urea electrooxidation.  $\text{M}^{3+}\text{OOH}$  reacts with  $\text{CO}(\text{NH}_2)_2$  and water molecules to produce  $\text{M}^{2+}(\text{OH})_2$ ,  $\text{N}_2$  and  $\text{CO}_2$ . For example, Tran reported the synthesis of a nanocomposite based on  $\text{CeO}_2$ -modified  $\text{LaNi}_{0.6}\text{Fe}_{0.4}\text{O}_3$  perovskite and MWCNT [75]. Niquel cations were responsible for the catalytic activity, while the  $\text{CeO}_2$  and multiwall carbon nanotubes imparted stability and increased the surface area, respectively. The authors report that the mechanism of electrochemical oxidation of urea is carried out in two steps, following the next reaction mechanism:



The urea detection level is of prime importance in clinical diagnosis and as a biomarker of the kidneys and liver functions. The most common methods for this important biomarker detection are UV-vis and infrared spectroscopy, ion and liquid chromatography-mass spectrometry, and fluorimetry [75–78]. Previously, the drawbacks of the enzymatic sensing of glucose, which are also applicable to urea, were mentioned. The typical amperometric urea biosensors are based upon the detection of ammonium ions resulting from the hydrolysis of urea in the presence of the enzyme urease viz. Due to the formation of ionic species by the reaction with the enzyme ( $\text{NH}_4^+$  and  $\text{HCO}_3^-$ ) in the presence of water, the electrochemical techniques become the suitable methodology for both the identification and quantification of urea. Thus, perovskite-based non-enzymatic detection systems for sensing analytes related to human kidney health were recently reported. Most of the studies have been focused on the improvement of (i) the surface area, (ii) imparting chemical stability, (iii) increasing the sensing performance, and (iv) reducing the cost of the fabrication of the sensor. For example, Tran et al. [75] used the perovskite of  $\text{LaNi}_{0.6}\text{Fe}_{0.4}\text{O}_3$  in a composite with  $\text{CeO}_2$  to improve the electro-oxidant activity towards urea. In addition, multi-wall carbon nanotubes (MWCNT) were included in the modified indium tin oxide (ITO) electrode, which improved the active electrochemical surface area. In the presence of urea, electrochemical oxidation is carried out by the reaction mechanism for the  $\text{Ni}^{2+}(\text{OH})_2/\text{Ni}^{3+}\text{OOH}$  pathway. Kumar et al. [79] reported the electrochemical detection of uric acid with a GP electrode modified with perovskite-type  $\text{XFeO}_3$  (with  $\text{X} = \text{La, Ce, Pr, Sm, Gd, Tb, and Dy}$ ). In every case, the perovskites were obtained in nanometric size with mainly cubic morphology in the 30 to 50 nm range. They found that the best charge transfer, using a standard  $[\text{Fe}(\text{CN})_6]^{-4}/[\text{Fe}(\text{CN})_6]^{-3}$  redox system, occurred when  $\text{X} = \text{La}$  with phosphate buffer

saline (PBS) electrolyte at a pH of five. The modified electrode was tested with human serum and urine samples, finding high precision in its application in clinical diagnosis. Another study for the detection of uric acid employed a graphite paste electrode modified with a neodymium ortho-ferrite perovskite ( $\text{NdFeO}_3$ ) to investigate the electrochemical behavior of the modified electrode. A standard  $[\text{Fe}(\text{CN})_6]^{-4}/[\text{Fe}(\text{CN})_6]^{-3}$  redox system was used and compared against the unmodified electrode (blank). The modified electrode showed an oxidation current almost three times higher than the blank, evidencing its greater efficiency in charge transport. This was verified in the determination of uric acid at a pH of five, employing cyclic voltammetry. The sensor showed high stability after 30 days and high reproducibility [80]. Nanocubes of  $\text{ZnSnO}_3$  perovskite, in its orthorhombic phase, were used for uric acid detection [81] by cyclic voltammetry and differential pulse voltammetry. Before analyte detection, a study to determine the optimal electrochemical surface-active area produced by the  $\text{ZnSnO}_3$  charge was carried out. It was determined that with 6  $\mu\text{L}$  of 0.5 wt% dispersion, an effective surface area of 0.1041  $\text{cm}^2$  was obtained, which favors the increment of the number of electrocatalytic active sites for redox reactions [81]. The detection of uric acid was attributed to the  $\text{Sn}^{2+}/\text{Sn}^{4+}$  oxidation states of tin, which favored the high electrochemical stability and sensor selectivity. Soundharraj et al. [82] reported urea sensing using a graphite electrode modified with zinc titanate ( $\text{ZnTiO}_3$ ) nanoparticles prepared by the sol-gel method. The modified electrode showed a peak current increase in the presence of urea compared to graphite alone. This was related to the transfer of electrons from the amine groups to the  $\text{ZnTiO}_3$  conduction band. The subsequent reduction in current with the increase in urea content was attributed to a delay in electrical conductivity due to an oxidation augment induced by the  $\text{TiO}_2$ . Chakraborty et al. [83] employed a mixture of cerium copper oxide ( $\text{CeCuO}_x$ ) and nickel oxide ( $\text{NiO}$ ) nanoparticles,  $\text{CeCuO}_x/\text{NiO}$ , for the detection of Lipocalin 2 (LCN2). LCN2 higher than standard levels may indicate various human health conditions, including kidney damage. Before the assembly of the silicon-based electrodes, a heat treatment was performed on the  $\text{CeCuO}_x$ , which was corroborated by cyclic voltammetry, showing that annealing at 800  $^\circ\text{C}$  produced the best electrochemical behavior. Subsequently, when adding the  $\text{NiO}$  nanoparticles, an improvement in the electrochemical activity was observed, which was explained first as an electronic transfer reaction from  $\text{CeCuO}_x$  to  $\text{NiO}$ , followed by a redox exchange reaction between  $\text{Fe}$ ,  $\text{Fe}^{3+/2+}$  in LCN2, and  $\text{Ni}^{3+/2+}$  of the  $\text{NiO}$  nanoparticles. The sensor showed high stability for 14 days and high selectivity in the presence of common interferents in human serum. In addition, high sensing precision was found when compared with human serum samples spiked with LCN2.

Perovskite-type transition metal oxides have high catalytic activities due to high electronic conductivities. Manna et al. modified a glassy carbon electrode with the composite rhenium oxide ( $\text{ReO}_3$ )/reduced graphene oxide (rGO) for uric acid detection. The high electrochemical response of the composite was attributed to the plasmonic behavior at the edges of the  $\text{ReO}_3$  nanostructure, which favors electron transfer. It was found that the presence of interfering species, such as glucose and some metal ions, does not significantly alter the detection of uric acid. This study also indicated that the modified electrode has good repeatability, so it can be applied to real samples. Analyses of synthetic human serum spiked with uric acid showed an acceptable recovery, in the order of 10%.

It should be noted that other works dedicated to electrochemical non-enzymatic sensing with perovskites have reported the detection of some of the analytes of interest in this section. However, in these studies, these compounds were only used as interferents [84,85]; therefore, they were not considered in this review.

### 3.3. Sensing of Hydrogen Peroxide ( $\text{H}_2\text{O}_2$ )

Hydrogen peroxide ( $\text{H}_2\text{O}_2$ ) is a reactive oxidant species (ROS) in all aerobic organisms [86,87]. It is a byproduct of aerobic metabolism and physiological processes such as immune activation [88], apoptosis [89], and cell growth [90]. Cells must remove this

molecule due to oxidized biological targets, causing different diseases and pathologies [88] like cancer [91], cell damage [92], and inflammatory diseases [93].

H<sub>2</sub>O<sub>2</sub> is not only a metabolic byproduct but also an oxidant reactive employed in food [94], pharmaceutical [95], cosmetics [96], and chemical industries [97]. Due to the relevance that H<sub>2</sub>O<sub>2</sub> represents, its quantification and detection become necessary. In the last decades, hydrogen peroxide sensors have been developed, mainly based on colorimetric [6], fluorescent [14], and electrochemical [98] methodologies. This last kind of sensor has attracted much attention due to its relative facility for developing commercial sensor devices. The reported electrochemical hydrogen peroxide sensor could be also enzymatic [99] or non-enzymatic [100]. The non-enzymatic sensor generally requires metal compounds that make the redox reaction for hydrogen peroxide detection. Perovskite-based materials are bimetallic compounds that show excellent electrochemical and redox properties. Conventionally, these materials were employed to explore the redox properties of perovskites to develop electrochemical sensors. The most applied conventional formula of perovskites to sense hydrogen peroxide is also the ABO<sub>3</sub> form. The most employed elements are from the lanthanide group or alkaline earth metals, where La, Sr, and Ca are the most important. Cations in B positions are usually transition metals from the fourth group of the periodic table, in which Ni, Co, Fe, and Mn are more frequently reported [101]. These cations (B) are responsible for interacting with hydrogen peroxide through the redox reaction B<sup>(M)+</sup>/B<sup>(M+1)+</sup>, producing molecular oxygen, water, and electrons as the responses of the electronic signal, which makes these substances electrochemically detectable and measurable. Due to lattice oxygen transfer, a redox mechanism occurs [64]. In contrast, the role of A cation is to stabilize the diverse B cation oxidation states in redox reactions. It has been reported that the general performance and redox behavior could be improved by partial substitution of A cations with the same element but with different oxidation states (A') [101]. The partial substitution of B with other cations with similar redox behaviors, B', is a strategy to improve redox efficiency [32].

The development of materials as non-enzymatic H<sub>2</sub>O<sub>2</sub> sensors has gone through several stages. The first studies focused on exploring different A cations and observing the electrocatalytic performance of these cations on H<sub>2</sub>O<sub>2</sub> decomposition. For example, the enthalpy of the formation of various perovskite copper oxides (ACuO<sub>3</sub>) with other A cations (A = La, Sr, Ba, Na, or K) and doped La<sub>1-x</sub>CuO<sub>3</sub> perovskite (where X = Ca, Sr, or Ba) requires higher exothermic oxidation energies than lanthanum nickelates and cobalt [102]. The research on the effect of cation A and possible dopant agents was complemented by varying the ratio of each cation and observing their effects. In perovskite oxides of La<sub>1-x</sub>Ca<sub>x</sub>MnO<sub>3</sub> (X = 0.0, 0.2, 0.4, and 0.6) using the citrate gel method, the concentration of calcium in perovskites affects the catalytic activity. This behavior is attributed to the non-stoichiometry  $\delta$ -oxygen and the average valence states of Mn responsible for the catalytic activity in the decomposition of hydrogen peroxide in an alkaline solution [101].

The methodology of perovskite oxide synthesis for H<sub>2</sub>O<sub>2</sub> detection has also been explored, where aspects such as the temperature of calcination and the effect on their crystalline structure (Figure 3) have been addressed by different research groups. For example, the catalytic redox activity of La<sub>1-x</sub>A<sub>x</sub>MnO<sub>3</sub> perovskite synthesized through denitrification using MW heating metal nitrate aqueous solutions doped with Ca and Pr and calcinated at 800 °C showed a crystal size larger than 48 nm. In contrast, the perovskites doped only with Ca exhibited a smaller crystal size but a surface area of 16 m<sup>2</sup> g<sup>-1</sup>. Nevertheless, the perovskite doped with Sr showed the most sensing sensitivity of H<sub>2</sub>O<sub>2</sub> [32]. The synthesis of La<sub>1-x</sub>Sr<sub>x</sub>MnO<sub>3</sub> perovskites by sol-gel methodology and calcinated between 550 and 750 °C for 5 h displayed considerable catalytic activity in an alkaline medium by reducing the analyte concentrations [103].

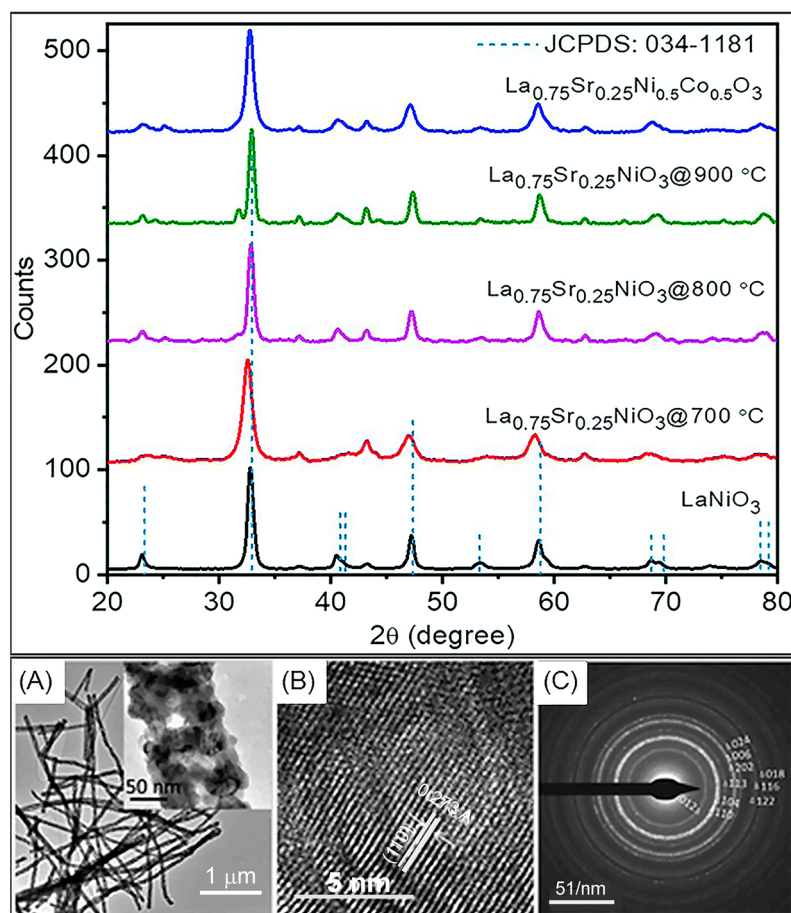


**Figure 3.** XRD of LaSrCrNiO representative patterns calcinated at 700, 800, 900, and 1000 °C. (A) TEM micrographs of perovskite fibers (magnified in the inset), (B) HRTEM lattice fringes, and (C) electron diffraction pattern. “Reprinted (Adapted) from reference [65]”.

The morphology of perovskites also plays a fundamental role in sensor development since this strategy impacts the superficial area of the electrode and, therefore, the active sites available for detection and sensing of the interest analytes. In this sense, the synthesis methodology is the most significant variable in the resulting morphology. Perovskite nanostructures have been synthesized by hydrothermal, solvothermal, and electrospinning routes, evidencing significant changes in their morphology and physicochemical properties. Thus, the same  $\text{CaTiO}_3$  system has been synthesized by several authors, evidencing a wide variety of morphologies ranging from butterfly-like dendrites [104], cubic particles [105], hollow micro-cubes [106], nanolamellate [107], and pyramids [82]. Also, a calcination procedure impacts the final morphology. For instance, electrospinning and sequential calcination of perovskite oxide  $\text{LaNiO}_3$  nanofibers reduced the fiber’s diameter from 400 to 140 nm. The corresponding amperometry sensor of  $\text{H}_2\text{O}_2$  and glucose developed with  $\text{LaNiO}_3$  nanofibers showed a fast response and long-term stability [31]. Likewise,  $\text{La}_{0.7}\text{Sr}_{0.3}\text{Mn}_{0.75}\text{Co}_{0.25}\text{O}_3$  nanofiber for sensing  $\text{H}_2\text{O}_2$  in alkaline buffer, synthesized through electrospinning and calcination, was produced as fibers with a diameter in the 250 to 300 nm range [108]. Other morphologies reported are nano brushes of  $\text{KNbO}_3$  synthesis by hydrothermal [109] and nano-structured perovskite oxide  $\text{LaNiTiO}$  [110]. Figure 4 displays a variety of morphologies reported in literature where different synthesis strategies were employed, intending to tailor the morphology of the obtained nanomaterial.

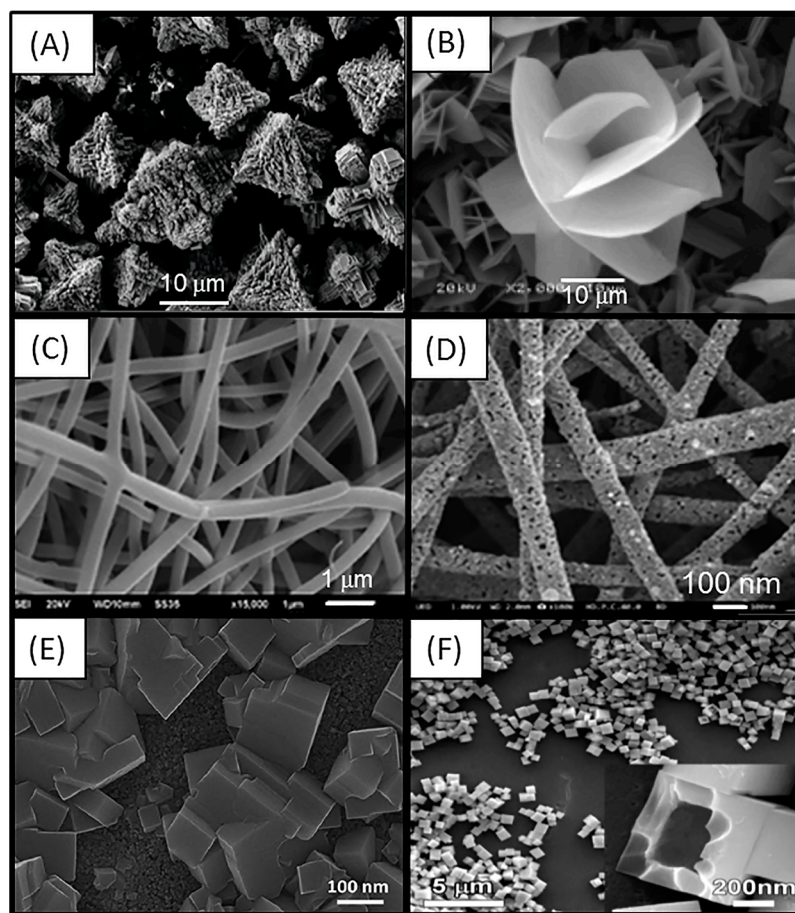


**Figure 4.** Morphology of perovskite-based materials (A) pyramids [82], (B) nanolamellate “Adapted with permission from {In situ hydrothermal synthesis of nanolamellate  $\text{CaTiO}_3$  with controllable structures and wettability, 46(19), Wang, D., Guo, Z., Chen, Y., Hao, J., & Liu, W.}. Copyright {2007} American Chemical Society [107].”, (C) nanofibers before calcination, reproduced from [65] with permission from Royal Society of Chemistry, (D) nanofibers after calcination, reproduced from reference [65] with permission of Royal Society of Chemistry, (E) nanocubes perovskites, reproduced from reference [108], and (F) hollow microcubes, adapted with permission from {Formation mechanism of  $\text{CaTiO}_3$  hollow crystals with different microstructures, 132(40), 14279–14287. Yang, X., Fu, J., Jin, C., Chen, J., Liang, C., Wu, M., & Zhou, W.}. Copyright {2010} American Chemical Society [106].

Interest in the investigation to develop new perovskite structures, combining different cations (A and B), doped or pure, to improve some properties of the sensor, such as the limit of detection, the linear range of detection, the sensitivity, and the selectivity, increased after 2009. I.e., two B cations and their ratios have been studied to improve the sensing properties of  $\text{LaCaBO}$  perovskites. They described the behavior of carbon electrodes loaded with  $\text{La}_{0.6}\text{Ca}_{0.4}\text{BO}_3$  ( $\text{B} = \text{Cr}, \text{Mn}, \text{Fe}, \text{Co}, \text{and Ni}$ ) perovskites oxides prepared by the amorphous malate precursor method, which provides a specific surface area in the range of  $8\text{--}30 \text{ m}^2/\text{g}$ . These values are considerably larger than those obtained by the conventional acetate decomposition method [21]. The potentiometric response of these perovskites was tested in the presence of  $\text{H}_2\text{O}_2$ , showing that material doped with Fe presented the best characteristics to develop a potentiometric sensor. Also, perovskite oxide  $\text{La}_x\text{Sr}_{1-x}\text{CoYFe}_1\text{-YO}_{3-\delta}$  was synthesized by the citrate method, and a comparison of its sensing properties showed that cobalt added to the ferrite structure enhanced the sensitivity, the linear range, and the detection limit [62]. Also,  $\text{SrFeO}_3$  perovskite doped with Ce showed that the presence of both cations improved the sensor performance [109]. A 3D macroporous  $\text{SmCoO}_3$  perovskite hydrogen peroxide sensor presented the lowest detection limit of  $0.004 \mu\text{M}$  and a linear detection in

the 0.1 to 10,000  $\mu\text{M}$  range, while the presence of glucose, ascorbic acid, dopamine, and uric acid did not show interference activity [110]. The properties of this sensor may be related to the hexagonally ordered microporous crystalline structure. Rare earth cuprate perovskites ( $\text{Ln}_2\text{CuO}_4$  where  $\text{Ln} = \text{Sm}$  or  $\text{La}$ ) were employed for sensing  $\text{H}_2\text{O}_2$  and presented broad detection ranges [111]. The perovskite with Sm exhibited a detection range of 1.24–35,440  $\mu\text{M}$ , while La showed a value of 0.50–23,350  $\mu\text{M}$  but a lower LOD. Additionally, the highest sensitivity sensor toward  $\text{H}_2\text{O}_2$  with a value of  $1667.9 \mu\text{A mM}^{-1} \text{cm}^{-2}$  was reported for a  $\text{La}_{0.9}\text{Sr}_{0.1}\text{NiO}_3$  nanofiber perovskite; this structure provides excellent ion transport channels and contact sites for the  $\text{H}_2\text{O}_2$  sensing [112].

Amperometric and potentiometric (cyclic voltammetry, CV) approaches are the most employed characterization techniques to evaluate the sensing capacity and electrocatalytic activity of perovskites. The way these electrochemical probes work is different. A potentiometric test measures the potential (voltage) between a working and reference electrode in a system with no significant current flow. The working electrode surface is modified so that changes in potential can be correlated with the changes in the analyte concentrations. The reference electrode remains constant, performing as a reference or comparison to the working electrode. Amperometric sensors rely on the principle that changes in current are related to changes in analyte concentration. In a typical CV experiment (Figure 5A), the determination and quantification of the analyte may be observed as a change in the anodic or cathodic peak current, which changes proportionally with the increase of the analyte concentration. On the other hand, amperometric recordings are performed by successive additions of the analyte and plotting the observed sensitivity to the analyte concentrations (Figure 5C). Consequently, it is possible to employ this technique as a parameter for sensing a variety of biomarkers.

Electrochemical impedance spectroscopy is another methodology for evaluating the electrocatalytic properties of perovskite-based materials. This technique is employed for analyzing interfacial events occurring at the electrode surface. The results are presented as a Nyquist plot (Figure 5B), where a semicircle reflecting the changes in the electron transfer resistance is displayed at high frequency. The charge transfer resistance ( $R_{ct}$ ) at the electrode interface is measured by the diameter of the semicircle, while the straight line at the low frequency corresponds to the dispersion process. An equivalent circuit is employed for fitting the impedance Nyquist plot. On the other hand, amperometric detection is carried out by fixing the potential at its oxidation or reduction peak potential value (previously determined from CV measurement) and monitoring its current response.

X-ray diffraction (XRD) is commonly employed to elucidate the perovskite crystalline structure. Ideally, perovskites of the form  $\text{ABX}_3$  are arranged into a cubic cell, where the atoms are just touching each other, and the B–X distance is equal to  $a/2$  and the A–X distance is  $2a/2$ , where  $a$  is the cube unit cell length and the relationship between radii of ions holds  $R_A + R_X = 2R_B + R_X$  [113–115]. However, distorted structures with tetragonal, rhombohedral, or orthorhombic symmetry have been found, mainly arising from smaller A ions that induce a tilting of the  $\text{BX}_6$  octahedra to optimize A–X bonding.  $\text{ABO}_3$  perovskites, where cation A is typically larger than cation B, are known to exhibit cubic, hexagonal, or even polytypism consisting of mixed cubic and hexagonal stacking of  $\text{AO}_3$  layers.

X-ray photoelectron spectroscopy (XPS) is also performed to probe the surface oxidation states and compositions, the binding energies, and the relative amounts of different metal and oxygen species on the surface available for the catalyst of the analyte. The characterization technique is also helpful in identifying the lattice oxygen species ( $\text{O}_2^-$ ), highly oxidative oxygen species ( $\text{O}_2^{2-}/\text{O}^-$ ), hydroxyl groups or the surface adsorbed oxygen ( $\text{HO}^-/\text{O}_2$ ), and adsorbed molecular water ( $\text{H}_2\text{O}$ ).

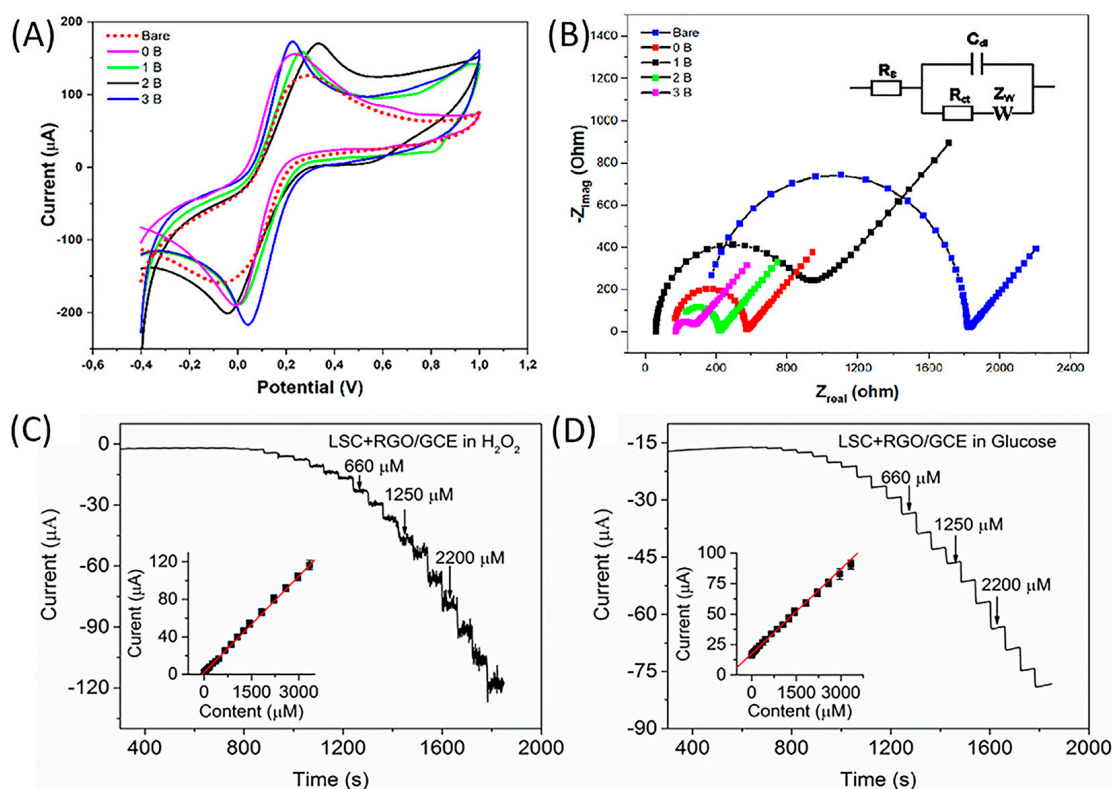


**Figure 5.** (A) Cyclic voltammogram measurements of  $\text{BaTi}_{0.7}\text{Fe}_{0.3}\text{O}_3\text{-NiFe}_2\text{O}_4$  nanocomposites conducted in a solution of standard redox probe of ferricyanide with the 5 mM in KCl as the supporting electrolyte for detection of  $\text{H}_2\text{O}_2$ . (B) Electrochemical impedance IS Nyquist spectra characterization of modified electrodes with the nanomaterials. Inset represents the modeled circuit that is used for curve fitting. "Reprinted (Adapted) from Construction and characterization of nanooval  $\text{BaTi}_{0.7}\text{Fe}_{0.3}\text{O}_3\text{@NiFe}_2\text{O}_4$  nanocomposites as an effective platform for the determination of  $\text{H}_2\text{O}_2$  Hammad, A.B.A., Magar, H.S., Mansour, A.M. et al. Copyright © 2023 [114]. (C) current-time responses of LSC + RGO/GCE upon addition of different concentrations of  $\text{H}_2\text{O}_2$  and (D) glucose in a 0.1 M NaOH electrolyte; insets show the linear range for  $\text{H}_2\text{O}_2$  and glucose detections. "Reprinted from High-performance non-enzymatic perovskite sensor for hydrogen peroxide and glucose electrochemical detection, 244, He, J., Sunarso, J., Zhu, Y., Zhong, Y., Miao, J., Zhou, W., & Shao, Z., Copyright (2017), with permission from Elsevier [64].

#### 4. Perspectives and Current Challenges

Although the use of perovskites as electrochemical sensors began in 1994, the challenge in recent years has undoubtedly been focused on improving the detection parameters of this type of sensor by electrocatalytic material modification. However, there are still areas of opportunity to obtain even lower detection limits or wider detection ranges, either through the development of new types of perovskites, composite materials, or variations in the sensor assembly. As can be inferred, the scientific interest in biomarker sensing through the development of perovskite-based sensors is notable, resulting in many reported perovskite systems. This review allowed a visualization of the effect of the modifications in the composition and crystal lattice of perovskites and the variations in the electrode assembly, which may result in systems with a better response to the sensing of analytes of interest. Table 1 summarizes some of the most critical parameters of electrochemical sensors, including the limit of detection (LOD), linear range of detection (LROD), and stability for the most frequently reported biomarkers, such as  $\text{H}_2\text{O}_2$ , uric acid, urea, and glucose. As observed from Table 1, the LOD for urea is close to 1  $\mu\text{M}$ , and the LROD is 25 to 650  $\mu\text{M}$ . For uric acid, these values are relatively smaller, with LOD in the range of

200–550 nM and LROD from 0.5 to 120  $\mu\text{M}$ . Regarding sensor stability, high stabilities are reported in the 15 to 45-day range.

**Table 1.** Summary of the sensing parameters of perovskites employed as non-enzymatic sensors of various biomarkers.

Perovskite Structure	Analyte	LOD ( $\mu\text{M}$ )	LROD ( $\mu\text{M}$ )	Interference	Year	Ref.
LaCuO <sub>3</sub> , LaSrCuO <sub>4</sub> , LaBaCuO <sub>4</sub> , NaCuO <sub>2</sub> , KCuO <sub>2</sub> .	H <sub>2</sub> O <sub>2</sub>	-	-	-	1994	[22]
La <sub>0.6</sub> Ca <sub>0.4</sub> Ni <sub>0.7</sub> Fe <sub>0.3</sub> O <sub>3</sub>	H <sub>2</sub> O <sub>2</sub>	0.5	0.1–1	-	1996	[28]
La <sub>0.66</sub> Sr <sub>0.33</sub> MnO <sub>3</sub>	H <sub>2</sub> O <sub>2</sub>	-	-	-	2009	[21]
La <sub>1-x</sub> Sr <sub>x</sub> MnO <sub>3</sub>	H <sub>2</sub> O <sub>2</sub>	-	-	-	2010	[23]
La <sub>1-x</sub> Ca <sub>x</sub> CoO <sub>3</sub>	H <sub>2</sub> O <sub>2</sub>	-	-	-	2012	[19]
LaNiTiO <sub>3</sub>	H <sub>2</sub> O <sub>2</sub>	0.01	0.05–1000	AA, DA, and UA	2013	[27]
LaNiO <sub>3</sub>	H <sub>2</sub> O <sub>2</sub>	0.32	0.05–1000	AA, DA, and UA	2013	[24]
KNbO <sub>3</sub>	H <sub>2</sub> O <sub>2</sub>	12	-	-	2014	[26]
La <sub>0.6</sub> Sr <sub>0.4</sub> Co <sub>0.2</sub> Fe <sub>0.8</sub> O <sub>3-<math>\delta</math></sub>	H <sub>2</sub> O <sub>2</sub>	5	0–3000	AA, DA, and UA	2015	[29]
La <sub>0.7</sub> Sr <sub>0.3</sub> Mn <sub>0.75</sub> Co <sub>0.25</sub> O <sub>3</sub>	H <sub>2</sub> O <sub>2</sub>	0.17	0.5–1000	AA, DA, and UA	2015	[25]
Ce doped SrFeO <sub>3</sub>	H <sub>2</sub> O <sub>2</sub>	10	0–500	Glu, CA, Na, NO <sub>2</sub> , Ca, N, Cu, Fe.	2016	[30]
LaNi <sub>0.6</sub> Co <sub>0.4</sub> O <sub>3</sub>	H <sub>2</sub> O <sub>2</sub>	0.05	0.2–3350	AA, DA, and UA	2017	[20]
SmCoO <sub>3</sub>	H <sub>2</sub> O <sub>2</sub>	0.004	0.1–10,000	Glu, AA, DA, and UA	2018	[31]
LaNiO <sub>3</sub>	H <sub>2</sub> O <sub>2</sub>	0.035	0.2–50, 50–3240	Suc, Glu, Fru, Ara, Urea, CA, L-Cys, Arg, APAP, and His.	2022	[34]
PrBaCo <sub>2</sub> O <sub>6</sub> (PBC), PrBaCo <sub>0.9</sub> Ni <sub>0.1</sub> O <sub>6-<math>\delta</math></sub> (PBCN)	H <sub>2</sub> O <sub>2</sub>	(0.17), (0.34)	5–6950, 5–6380	-	2022	[35]
La <sub>2</sub> CuO <sub>4</sub> Sm <sub>2</sub> CuO <sub>4</sub>	H <sub>2</sub> O <sub>2</sub>	(0.160), (0.410)	0.50–15.87 15.87–23,350 1.24–37.20 37.20–35,440	Glu, AA, UA, L-Cys, and TrTrp	2022	[32]
La <sub>0.9</sub> Sr <sub>0.1</sub> NiO <sub>3</sub>	H <sub>2</sub> O <sub>2</sub>	0.018	1~7000	-	2023	[33]
LaNi <sub>0.6</sub> Fe <sub>0.4</sub> O-CeO <sub>2</sub>	Urea	1	25 to 670	Creatinine, AA, Glu, Na <sup>+</sup> , Mg <sup>+</sup> , SO <sub>4</sub> <sup>-2</sup>	2018	[75]
XFeO <sub>3</sub> X=La, Ni, Fe, Ce	Uric acid	For La = 0.2	0.5 to 120	-	2018	[79]
NdFeO <sub>3</sub>	Uric acid	0.35	1 to 120	-	2019	[80]
ZnSnO <sub>3</sub>	Uric acid	0.550	1 to 5	Ca <sup>2+</sup> , Cl <sup>-</sup> , Na <sup>+</sup> , K <sup>+</sup> , Glu, and AA	2020	[81]
CaTiO <sub>3</sub>	Urea	1.6	50 to 450	AA, H <sub>2</sub> O <sub>2</sub> , UA, catechol, resorcinol, phenol, DA, and Glu	2020	[82]
ZnTiO <sub>3</sub>	Urea	76.16	30 to 150	-	2021	[83]
NiO/CeCuO <sub>x</sub>	Lipocalin	4.23 ng mL <sup>-1</sup>	25 to 400 ng mL <sup>-1</sup>	Crt, AA, human serum albumin (HSA), and hemoglobin (Hb)	2021	[115]
ReO <sub>3</sub>	Uric acid	0.06	1–10.5	Glu, Fe <sup>3+</sup> , Cys, Pb <sup>2+</sup> , Cd <sup>2+</sup> , and Cu <sup>2+</sup>	2022	[116]
La <sub>0.6</sub> Sr <sub>0.4</sub> CoO <sub>3</sub>	Glucose	0.05	2–3350	DA, UA, and AA	2017	[64]
LaSrCoNiO	Glucose	83	100–1000	Glu, Fru, Lac, Gal, Man, DA, and AA	2022	[65]
CsPbBr <sub>3</sub>	Glucose	0.8	2.0 to 170.0	Glu, Gly, Val, Glut, Cys, Mal, Lac, Man, Fru, and Suc	2022	[69]
CeAlO <sub>3</sub>	Glucose	0.00086	0.01–1034.5	NO <sub>3</sub> , NO <sub>2</sub> , H <sub>2</sub> O <sub>2</sub> , FA, UA, AA, PA, DA, Epi, CPF, and NFA	2021	[66]
LaCoO <sub>3</sub>	Glucose	0.0016	0.01–407.2	-	2021	[117]

Table 1. Cont.

Perovskite Structure	Analyte	LOD ( $\mu\text{M}$ )	LROD ( $\mu\text{M}$ )	Interference	Year	Ref.
$\text{SrTiO}_3$	Glucose	-	0–32,000	NaCl, DA, UA, AA, Suc	2021	[67]
$\text{Pr}_{1.9}\text{Ba}_{0.08}\text{Ni}_{0.95}\text{Zn}_{0.05}\text{O}_{4+\delta}$	Glucose	0.5	1.5 $\mu\text{M}$ –7000	-	2020	[118]
$\text{Sr}_2\text{PdO}_3$	Glucose	0.0021	0.2–100	UA, AA, and DA	2019	[58]
$\text{NdNiO}_3$	Glucose	0.3	0.5 to 4600	AA, DA, UA, Chol, Lac, Fru, Suc, NaCl, KCl, $\text{NO}_2$ , and $\text{Na}_2\text{SO}_4$	2017	[60]
$\text{CaTiO}_3$	Glucose	2.3	0.7 to 1490	UA and AA	2017	[69]
$\text{Sr}_{1.7}\text{Ca}_{0.3}\text{PdO}_3$	Glucose	0.0845	5 to 5600	-	2016	
$\text{LaTiO}_3$	Glucose	0.0000025	0.01 to 1000	Gly, Fruc, Mal, UU, AA, DP, $\text{Cu}^{2+}$ , $\text{Na}^+$ , $\text{Fe}^{3+}$ , $\text{Mn}^{2+}$ , and $\text{SO}_4^{2-}$	2015	[70]
$\text{SrPdO}_3$	Glucose	10.1	100–6000	UA, AA, DA, and PA	2015	[119]
$\text{La}_{0.88}\text{Sr}_{0.12}\text{MnO}_3$	Glucose	-	0.05–100	AA, UA, and DA	2015	[120]
$\text{La}_x\text{Sr}_{1-x}\text{Co}_y\text{Fe}_{1-y}\text{O}_{3-\delta}$	Glucose	5	0–200	AA, UA, and DA	2014	[62]
$\text{LiNbO}_3$	Glucose	10	300 to 3300	UA and AA	2014	[11]
$\text{LaNb}_2\text{O}_7$	Glucose	20	25 to 2830	-	2014	[10]
$\text{LaTiO}_3$	Glucose	0.21	2.5 to 4000	AA, UA, and DA	2013	[59]

AA = Ascorbic acid, UA = Uric acid, DA = Dopamine, PA = Paracetamol, L-cys = L-cysteine, Arg = Arginine, TrTrp = Tryptophan, CA = Citric acid, Chol = Cholesterol, Lac = Lactose, Fruc = Fructose, Mal = Maltose, Man = Mannose, Val = Valine, Glut = Glutamate, Gal = Galactose, Suc = Sucrose, CPF = Ciprofloxacin, NFA = Norfloxacin, Epi = Epinephrine, Gly = Glycine, Crt = Creatinine, HAS = Human serum albumin, Hb = Hemoglobin.

The monitoring of biomarkers is an essential tool for the prevention and control of patients with renal dysfunction or critical kidney disease. In this sense, the development of accurate devices for the detection of biomarkers is of high interest. Perovskite-based material is a versatile and promising candidate with desirable features for biomedical applications such as high selectivity and sensitivity, while providing stability to sensors. Additionally, these materials have tunable redox properties, high oxygen mobility, electronic and ionic conduction, and thermal and chemical stability. However, some significant challenges need to be addressed before these nanomaterials can be converted into real devices for patients who require a daily care control. Firstly, most of the sensors have been studied from the point of view of material science research, instead of meeting real specifications of this field that involve the treatment of biological fluid samples. For example, blood glucose concentrations in healthy people have been established to be 5.6 mM; however, for diabetic patients, values up to 7 mM can be expected. Although most of the investigation works presented an adequate LOD, most of them require extending their working range to fit the needs of correct blood glucose evaluation. Another key challenge is the fact that an alkaline electrolyte is required for the oxidation of several biomarkers, which does not correspond with the pH of the biological fluids.

Some areas of opportunity were detected, such as extending research related to other important biomarkers for renal health care, such as creatine and creatinine, which to our knowledge have not been explored yet for the perovskite-based materials. In this sense, as mentioned above, work on the development of non-enzymatic sensors for the detection of biomarkers of kidney health is still in its infancy; consequently, a trend in the type of metals used has not yet been observed in the general  $\text{ABO}_3$  structure, which is the most favorable for this purpose, although Fe seems to be the most used. However, we would have to wait a longer time to have more data to give a more objective conclusion.

## 5. Conclusions

Glucose, hydrogen peroxide, and non-protein nitrogenous compounds (NPNC), such as urea and uric acid, are important biomarkers of human kidney health. Acute kidney injury (AKI) in critically ill patients represents a risk factor for morbidity and mortality worldwide. Non-enzymatic detection tools have emerged as promising alternatives to

prevent and control critical diseases as they are quick to read, easy to use, and low-cost. In this work, relevant literature related to the non-enzymatic sensing of perovskite-based materials has been reviewed. Although the development of perovskite-based sensors is broad, as evidenced by the significant number of papers published, the works analyzed in the present review allow visualizing modifications implemented as strategies to increase the sensing performance. This results in better responses to the detection and quantification of different analytes. In general, in perovskite-based materials, catalytic activity and, therefore, sensing capacity largely depends on three relevant parameters: (i) the creation of a high surface area, small grain size, or a porous surface; (ii) the formation of oxygen vacancies; and (iii) the corresponding stoichiometry of A and B cations in the  $ABO_3$  chemical structure. Finally, it should be highlighted that the effect of modifications in perovskite composition and lattice and variations in electrode assembly became apparent. This allowed the progress of systems with a better response to detecting analytes of interest. However, the road to detection systems with higher efficiencies still has a long way to go. Among the most evident topics for future improvements are the use and synthesis of new perovskites, composites with carbon-based porous conductive materials, and variations in the sensor assembly.

**Author Contributions:** Conceptualization, E.A.Z.-C., C.I.P.-B., A.S.C.-D., M.C.M.-O. and C.L.-P.; investigation, E.A.Z.-C., C.I.P.-B., A.S.C.-D. and C.L.-P.; resources, E.A.Z.-C.; writing—original draft preparation, E.A.Z.-C., C.I.P.-B., A.E.-M., S.Y.R.-L. and C.L.-P.; writing—review and editing, E.A.Z.-C., C.I.P.-B. and C.L.-P.; supervision, E.A.Z.-C.; project administration, E.A.Z.-C.; funding acquisition, E.A.Z.-C. All authors have read and agreed to the published version of the manuscript.

**Funding:** This research was funded by the Centro de Investigación en Materiales Avanzados, S.C. (CIMAV).

**Institutional Review Board Statement:** Not applicable.

**Informed Consent Statement:** Not applicable.

**Data Availability Statement:** Not applicable.

**Acknowledgments:** We wish to thank CONAHCYT for the assignment of a Researcher position of the “Investigadores por México Program” for the project “Desarrollo de plataformas de sensores químicos para detección de creatinina” awarded to Claudia Ivone Piñón-Balderrama (CVU 387600).

**Conflicts of Interest:** The authors declare no conflict of interest.

## References

1. Cruz, D.N.; Bagshaw, S.M.; Maisel, A.; Lewington, A.; Thadhani, R.; Chakravarthi, R.; Murray, P.T.; Mehta, R.L.; Chawla, L.S. Use of Biomarkers to Assess Prognosis and Guide Management of Patients with Acute Kidney Injury. *Contrib. Nephrol.* **2013**, *182*, 45–64. [[CrossRef](#)] [[PubMed](#)]
2. Berl, T. American Society of Nephrology Renal Research Report. *J. Am. Soc. Nephrol.* **2005**, *16*, 1886–1903. [[CrossRef](#)]
3. Hojs, N.V.; Bevc, S.; Ekart, R.; Hojs, R. Oxidative Stress Markers in Chronic Kidney Disease with Emphasis on Diabetic Nephropathy. *Antioxidants* **2020**, *9*, 925. [[CrossRef](#)] [[PubMed](#)]
4. Wen, L.; Li, Y.; Li, S.; Hu, X.; Wei, Q.; Dong, Z. Glucose Metabolism in Acute Kidney Injury and Kidney Repair. *Front. Med.* **2021**, *8*, 744122. [[CrossRef](#)] [[PubMed](#)]
5. Geleta, G.S. A Colorimetric Aptasensor Based on Two Dimensional (2D) Nanomaterial and Gold Nanoparticles for Detection of Toxic Heavy Metal Ions: A Review. *Food Chem. Adv.* **2023**, *2*, 100184. [[CrossRef](#)]
6. Kailasa, S.K.; Vajubhai, G.N.; Koduru, J.R.; Park, T.J. Recent Progress of Nanomaterials for Colorimetric and Fluorescence Sensing of Reactive Oxygen Species in Biological and Environmental Samples. *Trends Environ. Anal. Chem.* **2023**, *37*, e00196. [[CrossRef](#)]
7. Yang, L.; Janie, E.; Huang, T.; GHzen, J.; Kissinger, P.T.; Vreeke, M.; Heller, A. Applications of “Wired” Peroxidase Electrodes for Peroxide Determination in Liquid Chromatography Coupled to Oxidase Immobilized Enzyme Reactors. *Anal. Chem.* **1995**, *67*, 1326–1331. [[CrossRef](#)]
8. Turner, A.; Karube, I.; Wilson, G.S. *Biosensors: Fundamentals and Applications*; Oxford University Press: New York, NY, USA, 2019; ISBN 9783110641080.
9. Narang, J.; Pundir, C.S. *Biosensors: An Introductory Textbook*; Pan Stanford Publishing Pte, Ltd.: Singapore, 2017; ISBN 978-1-315-15652-1.
10. Zhang, X.; Shen, L.; Wang, M.; Siqin, G.; Tong, Z.; Xu, R.; Zhang, D.; Ma, J.; Liu, L. A Novel Glucose Biosensor Constructed by Glucose Oxidase Immobilized with Methylene Blue Intercalated Layered Lanthanum Niobic Acid Nanocomposite. *Mater. Lett.* **2014**, *135*, 39–42. [[CrossRef](#)]

11. Cai, B.; Zhao, M.; Ma, Y.; Ye, Z.; Huang, J. Bio-Inspired Formation of Mesoporous LiNbO<sub>3</sub> Nanotubes and Application for Glucose Biosensor. *Electrochim. Acta* **2014**, *147*, 176–182. [[CrossRef](#)]
12. Park, S.; Boo, H.; Chung, T.D. Electrochemical Non-Enzymatic Glucose Sensors. *Anal. Chim. Acta* **2006**, *556*, 46–57. [[CrossRef](#)]
13. Chen, L.; Yang, J.; Chen, W.; Sun, S.; Tang, H.; Li, Y. Perovskite Mesoporous LaFeO<sub>3</sub> with Peroxidase-like Activity for Colorimetric Detection of Gallic Acid. *Sens. Actuators B Chem.* **2020**, *321*, 128642. [[CrossRef](#)]
14. Xu, W.; Li, F.; Cai, Z.; Wang, Y.; Luo, F.; Chen, X. An Ultrasensitive and Reversible Fluorescence Sensor of Humidity Using Perovskite CH<sub>3</sub>NH<sub>3</sub>PbBr<sub>3</sub>. *J. Mater. Chem. C* **2016**, *4*, 9651–9655. [[CrossRef](#)]
15. George, J.; Halali, V.V.; Sanjayan, C.G.; Suvina, V.; Sakar, M.; Balakrishna, R.G. Perovskite Nanomaterials as Optical and Electrochemical Sensors. *Inorg. Chem. Front.* **2020**, *7*, 2702–2725. [[CrossRef](#)]
16. Cardoso, A.G.; Viltres, H.; Ortega, G.A.; Phung, V.; Grewal, R.; Mozaffari, H.; Ahmed, S.R.; Rajabzadeh, A.R.; Srinivasan, S. Electrochemical Sensing of Analytes in Saliva: Challenges, Progress, and Perspectives. *TrAC-Trends Anal. Chem.* **2023**, *160*, 116965. [[CrossRef](#)]
17. Wang, Y.; Wang, X.; Lu, W.; Yuan, Q.; Zheng, Y.; Yao, B. A Thin Film Polyethylene Terephthalate (PET) Electrochemical Sensor for Detection of Glucose in Sweat. *Talanta* **2019**, *198*, 86–92. [[CrossRef](#)] [[PubMed](#)]
18. Liu, J.; Lu, W.; Zhang, L.; Yang, J.; Yao, Z.P.; He, Y.; Li, Y. Integrated Hand-Held Electrochemical Sensor for Multicomponent Detection in Urine. *Biosens. Bioelectron.* **2021**, *193*, 113534. [[CrossRef](#)] [[PubMed](#)]
19. Wang, Y.R.; Chuang, H.C.; Tripathi, A.; Wang, Y.L.; Ko, M.L.; Chuang, C.C.; Chen, J.C. High-Sensitivity and Trace-Amount Specimen Electrochemical Sensors for Exploring the Levels of  $\beta$ -Amyloid in Human Blood and Tears. *Anal. Chem.* **2021**, *93*, 8099–8106. [[CrossRef](#)] [[PubMed](#)]
20. Yang, L.; Yang, J.; Dong, Q.; Zhou, F.; Wang, Q.; Wang, Z.; Huang, K.; Yu, H.; Xiong, X. One-Step Synthesis of CuO Nanoparticles Based on Flame Synthesis: As a Highly Effective Non-Enzymatic Sensor for Glucose, Hydrogen Peroxide and Formaldehyde. *J. Electroanal. Chem.* **2021**, *881*, 114965. [[CrossRef](#)]
21. Shimizu, Y.; Komatsu, H.; Michishita, S.; Miura, N.; Yamazo, N. Sensing Characteristics of Hydrogen Peroxide Sensor Using Carbon-Based Electrode Loaded with Perovskite-Type Oxide. *Sens. Actuators B Chem.* **1996**, *34*, 493–498. [[CrossRef](#)]
22. Li, Z.; Meng, M.; Li, Q.; Xie, Y.; Hu, T.; Zhang, J. Fe-Substituted Nanometric La<sub>0.9</sub>K<sub>0.1</sub>CoxFexO<sub>3- $\delta$</sub>  Perovskite Catalysts Used for Soot Combustion, NO<sub>x</sub> Storage and Simultaneous Catalytic Removal of Soot and NO<sub>x</sub>. *Chem. Eng. J.* **2010**, *164*, 98–105. [[CrossRef](#)]
23. Li, C.L.; Jiang, B.S.; Fanchiang, W.L.; Lin, Y.C. The Effect of Pd Content in LaMnO<sub>3</sub> for Methanol Partial Oxidation. *Catal. Commun.* **2011**, *16*, 165–169. [[CrossRef](#)]
24. Li, C.L.; Wang, C.L.; Lin, Y.C. Pd-Integrated Lanthanum-Transition Metal Perovskites for Methanol Partial Oxidation. *Catal. Today* **2011**, *174*, 135–140. [[CrossRef](#)]
25. Atfield, J.P. “A” Cation Control of Perovskite Properties. *Cryst. Eng.* **2002**, *5*, 427–438. [[CrossRef](#)]
26. King, G.; Woodward, P.M. Cation Ordering in Perovskites. *J. Mater. Chem.* **2010**, *20*, 5785–5796. [[CrossRef](#)]
27. Garibay-Alvarado, J.A.; Fariás, R.; Reyes-López, S.Y. Sol-Gel and Electrospinning Synthesis of Lithium Niobate-Silica Nanofibers. *Coatings* **2019**, *9*, 212. [[CrossRef](#)]
28. Kobylanskaya, S.D.; Gavrilenko, O.N.; Belous, A.G. Synthesis of Nanosized (Li,La){Ti,Nb,Ta}O<sub>3</sub> Particles Using the Sol-Gel Method. *Russ. J. Inorg. Chem.* **2013**, *58*, 637–643. [[CrossRef](#)]
29. Masloboeva, S.M.; Palatnikov, M.N.; Arutyunyan, L.G. Sol-Gel Synthesis of a Zn-Doped Lithium Tantalate Growth Charge. *Inorg. Mater.* **2020**, *56*, 270–276. [[CrossRef](#)]
30. Mudra, E.; Brunckova, H.; Streckova, M.; Sopcak, T.; Sebek, M.; Durisin, J.; Girman, V.; Dusza, J. Preparation and Characterization of Ceramic Nanofibers Based on Lanthanum Tantalates. *J. Sol-Gel Sci. Technol.* **2016**, *78*, 322–330. [[CrossRef](#)]
31. Wang, B.; Gu, S.; Ding, Y.; Chu, Y.; Zhang, Z.; Ba, X.; Zhang, Q.; Li, X. A Novel Route to Prepare LaNiO<sub>3</sub> Perovskite-Type Oxide Nanofibers by Electrospinning for Glucose and Hydrogen Peroxide Sensing. *Analyst* **2013**, *138*, 362–367. [[CrossRef](#)]
32. Luque, G.L.; Ferreyra, N.F.; Leyva, A.G.; Rivas, G.A. Characterization of Carbon Paste Electrodes Modified with Manganese Based Perovskites-Type Oxides from the Amperometric Determination of Hydrogen Peroxide. *Sens. Actuators B Chem.* **2009**, *142*, 331–336. [[CrossRef](#)]
33. Xu, X.; Zhong, Y.; Shao, Z. Double Perovskites in Catalysis, Electrocatalysis, and Photo(Electro)Catalysis. *Trends Chem.* **2019**, *1*, 410–424. [[CrossRef](#)]
34. Grimaud, A.; May, K.J.; Carlton, C.E.; Lee, Y.L.; Risch, M.; Hong, W.T.; Zhou, J.; Shao-Horn, Y. Double Perovskites as a Family of Highly Active Catalysts for Oxygen Evolution in Alkaline Solution. *Nat. Commun.* **2013**, *4*, 2439. [[CrossRef](#)] [[PubMed](#)]
35. Kim, G.; Wang, S.; Jacobson, A.J.; Reimus, L.; Brodersen, P.; Mims, C.A. Rapid Oxygen Ion Diffusion and Surface Exchange Kinetics in PrBaCo<sub>2</sub>O<sub>5+x</sub> with a Perovskite Related Structure and Ordered a Cations. *J. Mater. Chem.* **2007**, *17*, 2500–2505. [[CrossRef](#)]
36. Chen, D.; Ran, R.; Zhang, K.; Wang, J.; Shao, Z. Intermediate-Temperature Electrochemical Performance of a Polycrystalline PrBaCo<sub>2</sub>O<sub>5+ $\delta$</sub>  Cathode on Samarium-Doped Ceria Electrolyte. *J. Power Sources* **2009**, *188*, 96–105. [[CrossRef](#)]
37. Shellaiiah, M.; Sun, K.W. Review on Sensing Applications of Perovskite Nanomaterials. *Chemosensors* **2020**, *8*, 55. [[CrossRef](#)]
38. Wang, W.; Pang, S.; Su, Y.; Shen, X.; Wang, Y.; Xu, K.; Xi, X.; Xiang, J. The Effect of Calcium on the Properties of SmBa<sub>1-x</sub>CaxCoCuO<sub>5+ $\delta$</sub>  as a Cathode Material for Intermediate-Temperature Solid Oxide Fuel Cells. *J. Eur. Ceram. Soc.* **2017**, *37*, 1557–1562. [[CrossRef](#)]
39. Yoo, S.; Jun, A.; Ju, Y.W.; Odkhuu, D.; Hyodo, J.; Jeong, H.Y.; Park, N.; Shin, J.; Ishihara, T.; Kim, G. Development of Double-Perovskite Compounds as Cathode Materials for Low-Temperature Solid Oxide Fuel Cells. *Angew. Chemie-Int. Ed.* **2014**, *53*, 13064–13067. [[CrossRef](#)]

40. West, M.; Manthiram, A. Layered  $\text{LnBa}_{1-x}\text{Sr}_x\text{CoCuO}_{5+\delta}$  ( $\text{Ln} = \text{Nd}$  and  $\text{Gd}$ ) Perovskite Cathodes for Intermediate Temperature Solid Oxide Fuel Cells. *Int. J. Hydrogen Energy* **2013**, *38*, 3364–3372. [[CrossRef](#)]
41. Jun, A.; Kim, J.; Shin, J.; Kim, G. Optimization of Sr Content in Layered  $\text{SmBa}_{1-x}\text{Sr}_x\text{Co}_{2.0}\text{O}_{5+\delta}$  Perovskite Cathodes for Intermediate-Temperature Solid Oxide Fuel Cells. *Int. J. Hydrogen Energy* **2012**, *37*, 18381–18388. [[CrossRef](#)]
42. He, J.; Xu, X.; Li, M.; Zhou, S.; Zhou, W. Recent Advances in Perovskite Oxides for Non-Enzymatic Electrochemical Sensors: A Review. *Anal. Chim. Acta* **2023**, *1251*, 341007. [[CrossRef](#)]
43. Burke, L.D.; Lyons, M.E.G. Electrochemistry of Hydrous Oxide Films. *Mod. Asp. Electrochem.* **1986**, *18*, 169–248. [[CrossRef](#)]
44. Mefford, J.T.; Rong, X.; Abakumov, A.M.; Hardin, W.G.; Dai, S.; Kolpak, A.M.; Johnston, K.P.; Stevenson, K.J. Water Electrolysis on  $\text{La}_{1-x}\text{Sr}_x\text{CoO}_{3-\delta}$  Perovskite Electrocatalysts. *Nat. Commun.* **2016**, *7*, 11053. [[CrossRef](#)] [[PubMed](#)]
45. Gao, W.; Zhu, Y.; Wang, Y.; Yuan, G.; Liu, J.M. A Review of Flexible Perovskite Oxide Ferroelectric Films and Their Application. *J. Mater.* **2020**, *6*, 1–16. [[CrossRef](#)]
46. Rørvik, P.M.; Grande, T.; Einarsrud, M.A. One-Dimensional Nanostructures of Ferroelectric Perovskites. *Adv. Mater.* **2011**, *23*, 4007–4034. [[CrossRef](#)] [[PubMed](#)]
47. Bhaumik, S.; Ray, S.; Batabyal, S.K. Recent Advances of Lead-Free Metal Halide Perovskite Single Crystals and Nanocrystals: Synthesis, Crystal Structure, Optical Properties, and Their Diverse Applications. *Mater. Today Chem.* **2020**, *18*, 100363. [[CrossRef](#)]
48. Adinolfi, V.; Peng, W.; Walters, G.; Bakr, O.M.; Sargent, E.H. The Electrical and Optical Properties of Organometal Halide Perovskites Relevant to Optoelectronic Performance. *Adv. Mater.* **2018**, *30*, 1700764. [[CrossRef](#)] [[PubMed](#)]
49. Qiao, Y.; Liu, Q.; Lu, S.; Chen, G.; Gao, S.; Lu, W.; Sun, X. High-Performance Non-Enzymatic Glucose Detection: Using a Conductive Ni-MOF as an Electrocatalyst. *J. Mater. Chem. B* **2020**, *8*, 5411–5415. [[CrossRef](#)] [[PubMed](#)]
50. Clark, L.C.; Lyons, C. Electrode Systems for Continuous Monitoring in Cardiovascular Surgery. *Ann. N. Y. Acad. Sci.* **1962**, *102*, 29–45. [[CrossRef](#)]
51. Wang, J. Electrochemical Glucose Biosensors. *Electrochem. Sensors, Biosens. their Biomed. Appl.* **2008**, *108*, 814–825. [[CrossRef](#)]
52. Rocchitta, G.; Spanu, A.; Babudieri, S.; Latte, G.; Madeddu, G.; Galleri, G.; Nuvoli, S.; Bagella, P.; Demartis, M.I.; Fiore, V.; et al. Enzyme Biosensors for Biomedical Applications: Strategies for Safeguarding Analytical Performances in Biological Fluids. *Sensors* **2016**, *16*, 780. [[CrossRef](#)] [[PubMed](#)]
53. Dzyadevych, S.V.; Arkhypova, V.N.; Soldatkin, A.P.; El'skaya, A.V.; Martelet, C.; Jaffrezic-Renault, N. Amperometric Enzyme Biosensors: Past, Present and Future. *Itbm-Rbm* **2008**, *29*, 171–180. [[CrossRef](#)]
54. Wang, Y.; Xu, Y.; Luo, L.; Ding, Y.; Liu, X. Preparation of Perovskite-Type Composite Oxide  $\text{LaNi}_{0.5}\text{Ti}_{0.5}\text{O}_3\text{-NiFe}_2\text{O}_4$  and Its Application in Glucose Biosensor. *J. Electroanal. Chem.* **2010**, *642*, 35–40. [[CrossRef](#)]
55. George, G.; Ede, S.R.; Luo, Z. *Fundamentals of Perovskite Oxides: Synthesis, Structure, Properties and Applications*; CRC Press: Boca Raton, FL, USA, 2020.
56. Boubezari, I.; Zazoua, A.; Errachid, A.; Jaffrezic-Renault, N. Sensitive Electrochemical Detection of Bioactive Molecules (Hydrogen Peroxide, Glucose, Dopamine) with Perovskites-Based Sensors. *Chemosensors* **2021**, *9*, 289. [[CrossRef](#)]
57. Natali Sora, I.; Caronna, T.; Fontana, F.; De Julián Fernández, C.; Caneschi, A.; Green, M. Crystal Structures and Magnetic Properties of Strontium and Copper Doped Lanthanum Ferrites. *J. Solid State Chem.* **2012**, *191*, 33–39. [[CrossRef](#)]
58. Atta, N.F.; Galal, A.; El-Ads, E.H. Effect of B-Site Doping on  $\text{Sr}_2\text{PdO}_3$  Perovskite Catalyst Activity for Non-Enzymatic Determination of Glucose in Biological Fluids. *J. Electroanal. Chem.* **2019**, *852*, 113523. [[CrossRef](#)]
59. Wang, Y.Z.; Zhong, H.; Li, X.M.; Jia, F.F.; Shi, Y.X.; Zhang, W.G.; Cheng, Z.P.; Zhang, L.L.; Wang, J.K. Perovskite  $\text{LaTiO}_3\text{-Ag}_{0.2}$  Nanomaterials for Nonenzymatic Glucose Sensor with High Performance. *Biosens. Bioelectron.* **2013**, *48*, 56–60. [[CrossRef](#)]
60. Sivakumar, M.; Pandi, K.; Chen, S.M.; Cheng, Y.H.; Sakthivel, M. Facile Synthesis of Perovskite-Type  $\text{NdNiO}_3$  Nanoparticles for an Effective Electrochemical Non-Enzymatic Glucose Biosensor. *New J. Chem.* **2017**, *41*, 11201–11207. [[CrossRef](#)]
61. Wang, Y.; Xu, Y.; Luo, L.; Ding, Y.; Liu, X.; Huang, A. A Novel Sensitive Nonenzymatic Glucose Sensor Based on Perovskite  $\text{LaNi}_{0.5}\text{Ti}_{0.5}\text{O}_3$ -Modified Carbon Paste Electrode. *Sens. Actuators B Chem.* **2010**, *151*, 65–70. [[CrossRef](#)]
62. Liotta, L.F.; Puleo, F.; LaParola, V.; Leonardi, S.G.; Donato, N.; Aloisio, D.; Neri, G.  $\text{La}_{0.6}\text{Sr}_{0.4}\text{FeO}_{3-\delta}$  and  $\text{La}_{0.6}\text{Sr}_{0.4}\text{Co}_{0.2}\text{Fe}_{0.8}\text{O}_{3-\delta}$  Perovskite Materials for  $\text{H}_2\text{O}_2$  and Glucose Electrochemical Sensors. *Electroanalysis* **2015**, *27*, 684–692. [[CrossRef](#)]
63. El-Ads, E.H.; Galal, A.; Atta, N.F. The Effect of A-Site Doping in a Strontium Palladium Perovskite and Its Applications for Non-Enzymatic Glucose Sensing. *RSC Adv.* **2016**, *6*, 16183–16196. [[CrossRef](#)]
64. He, J.; Sunarso, J.; Zhu, Y.; Zhong, Y.; Miao, J.; Zhou, W.; Shao, Z. High-Performance Non-Enzymatic Perovskite Sensor for Hydrogen Peroxide and Glucose Electrochemical Detection. *Sens. Actuators B Chem.* **2017**, *244*, 482–491. [[CrossRef](#)]
65. Pelucarte, K.D.; Hatchell, T.A.; George, G.; Ede, S.R.; Adhikari, M.; Lin, Y.; Wen, J.; Luo, Z.; Han, S. Electrospun Porous La-Sr-Co-Ni-O Nanofibers for Highly Sensitive Non-Enzymatic Glucose Detection. *Mater. Adv.* **2022**, *3*, 2096–2103. [[CrossRef](#)]
66. Rajaji, U.; Ganesh, P.S.; Chen, S.M.; Govindasamy, M.; Kim, S.Y.; Alshgari, R.A.; Shimoga, G. Deep Eutectic Solvents Synthesis of Perovskite Type Cerium Aluminate Embedded Carbon Nitride Catalyst: High-Sensitive Amperometric Platform for Sensing of Glucose in Biological Fluids. *J. Ind. Eng. Chem.* **2021**, *102*, 312–320. [[CrossRef](#)]
67. Wang, Y.; Yin, L.; Wu, J.; Li, N.; He, N.; Zhao, H.; Wu, Q.; Li, X. Perovskite- $\text{SrTiO}_3/\text{TiO}_2/\text{PDA}$  as Photoelectrochemical Glucose Biosensor. *Ceram. Int.* **2021**, *47*, 29807–29814. [[CrossRef](#)]
68. Gao, M.; Li, J.; Qiu, L.; Xia, X.; Cheng, X.; Xu, F.; Xu, G.; Wei, F.; Yang, J.; Hu, Q.; et al. Glucose and PH Responsive Fluorescence Detection System Based on Simple Synthesis of Silicon-Coated Perovskite Quantum Dots. *Spectrochim. Acta-Part A Mol. Biomol. Spectrosc.* **2023**, *289*, 122212. [[CrossRef](#)]

69. Niu, X.; Gao, H.; Du, J. CsPbBr<sub>3</sub> Perovskite Nanocrystals Decorated with Cu Nanoclusters for Ratiometric Detection of Glucose. *ACS Appl. Nano Mater.* **2022**, *5*, 2350–2357. [CrossRef]
70. Jia, F.F.; Zhong, H.; Zhang, W.G.; Li, X.R.; Wang, G.Y.; Song, J.; Cheng, Z.P.; Yin, J.Z.; Guo, L.P. A Novel Nonenzymatic ECL Glucose Sensor Based on Perovskite LaTiO<sub>3</sub>-Ag<sub>0.1</sub> Nanomaterials. *Sens. Actuators B Chem.* **2015**, *212*, 174–182. [CrossRef]
71. Encyclopaedia Britannica. Urea. Chemical Compound. Encyclopaedia Britannica 2023. Available online: <https://www.britannica.com/science/urea> (accessed on 11 August 2023).
72. Sha, R.; Komori, K.; Badhulika, S. Graphene–Polyaniline Composite Based Ultra-Sensitive Electrochemical Sensor for Non-Enzymatic Detection of Urea. *Electrochim. Acta* **2017**, *233*, 44–51. [CrossRef]
73. Mondal, S.; Sangaranarayanan, M.V. A Novel Non-Enzymatic Sensor for Urea Using a Polypyrrole-Coated Platinum Electrode. *Sens. Actuators B Chem.* **2013**, *177*, 478–486. [CrossRef]
74. Mozaffari, S.A.; Rahmanian, R.; Abedi, M.; Amoli, H.S. Urea Impedimetric Biosensor Based on Reactive RF Magnetron Sputtered Zinc Oxide Nanoporous Transducer. *Electrochim. Acta* **2014**, *146*, 538–547. [CrossRef]
75. Tran, T.Q.N.; Yoon, S.W.; Park, B.J.; Yoon, H.H. CeO<sub>2</sub>-Modified LaNi<sub>0.6</sub>Fe<sub>0.4</sub>O<sub>3</sub> Perovskite and MWCNT Nanocomposite for Electrocatalytic Oxidation and Detection of Urea. *J. Electroanal. Chem.* **2018**, *818*, 76–83. [CrossRef]
76. Ezhilan, M.; Gumpu, M.B.; Ramachandra, B.L.; Nesakumar, N.; Babu, K.J.; Krishnan, U.M.; Rayappan, J.B.B. Design and Development of Electrochemical Biosensor for the Simultaneous Detection of Melamine and Urea in Adulterated Milk Samples. *Sens. Actuators B Chem.* **2017**, *238*, 1283–1292. [CrossRef]
77. Kumar, V.; Chopra, A.; Arora, S.; Yadav, S.; Kumar, S.; Kaur, I. Amperometric Sensing of Urea Using Edge Activated Graphene Nanoplatelets. *RSC Adv.* **2015**, *5*, 13278–13284. [CrossRef]
78. Verma, R.; Gupta, B.D. A Novel Approach for Simultaneous Sensing of Urea and Glucose by SPR Based Optical Fiber Multianalyte Sensor. *Analyst* **2014**, *139*, 1449–1455. [CrossRef] [PubMed]
79. Kumar, Y.; Pradhan, S.; Pramanik, S.; Bandyopadhyay, R.; Das, D.K.; Pramanik, P. Efficient Electrochemical Detection of Guanine, Uric Acid and Their Mixture by Composite of Nano-Particles of Lanthanides Ortho-Ferrite XFeO<sub>3</sub> (X = La, Gd, Pr, Dy, Sm, Ce and Tb). *J. Electroanal. Chem.* **2018**, *830–831*, 95–105. [CrossRef]
80. Kumar, Y.; Singh, P.P.; Pramanik, P.; Das, D. Electrochemical Determination of Guanine and Uric Acid Using NdFeO<sub>3</sub> Nps Modified Graphite Paste Electrode. *J. Sci. Ind. Res.* **2019**, *78*, 177–181.
81. Durai, L.; Badhulika, S. One Pot Hydrothermal Synthesis of Large Area Nano Cube like ZnSnO<sub>3</sub> Perovskite for Simultaneous Sensing of Uric Acid and Dopamine Using Differential Pulse Voltammetry. *IEEE Sens. J.* **2020**, *20*, 13212–13219. [CrossRef]
82. Ahmad, K.; Kumar, P.; Mobin, S.M. Hydrothermally Grown Novel Pyramids of the CaTiO<sub>3</sub> perovskite as an Efficient Electrode Modifier for Sensing Applications. *Mater. Adv.* **2020**, *1*, 2003–2009. [CrossRef]
83. Soundharraj, P.; Jagannathan, M.; Dhinasekaran, D.; Thiruvarasu, P. Fluorescent Zinc Titanate as an Effective Sensing Platform for Urea Detection. *Mater. Today Proc.* **2021**, *50*, 101–106. [CrossRef]
84. Atta, N.F.; Ali, S.M.; El-Ads, E.H.; Galal, A. The Electrochemistry and Determination of Some Neurotransmitters at SrPdO<sub>3</sub> Modified Graphite Electrode. *J. Electrochem. Soc.* **2013**, *160*, G3144–G3151. [CrossRef]
85. Atta, N.F.; Ali, S.M.; El-Ads, E.H.; Galal, A. Nano-Perovskite Carbon Paste Composite Electrode for the Simultaneous Determination of Dopamine, Ascorbic Acid and Uric Acid. *Electrochim. Acta* **2014**, *128*, 16–24. [CrossRef]
86. Marinho, H.S.; Real, C.; Cyrne, L.; Soares, H.; Antunes, F. Hydrogen Peroxide Sensing, Signaling and Regulation of Transcription Factors. *Redox Biol.* **2014**, *2*, 535–562. [CrossRef] [PubMed]
87. Meier, J.; Hofferber, E.; Stapleton, J.A.; Iverson, N.M. Hydrogen Peroxide Sensors for Biomedical Applications. *Chemosensors* **2019**, *7*, 64. [CrossRef]
88. Pravda, J. Hydrogen Peroxide and Disease: Towards a Unified System of Pathogenesis and Therapeutics. *Mol. Med.* **2020**, *26*, 1–10. [CrossRef]
89. Li, W.; Yin, X.; Yan, Y.; Liu, C.; Li, G. Kurarinone Attenuates Hydrogen Peroxide-Induced Oxidative Stress and Apoptosis through Activating the PI3K/Akt Signaling by Upregulating IGF1 Expression in Human Ovarian Granulosa Cells. *Environ. Toxicol.* **2023**, *38*, 28–38. [CrossRef] [PubMed]
90. Song, K.E.; Hwang, H.R.; Hong, E.S.H.; Konvalina, P.; Jun, W.J.; Jung, J.W.; Shim, S. Hydrogen Peroxide Ameliorates the Adversities of Drought Stress during Germination and Seedling Growth in Sorghum (*Sorghum Bicolor* L.). *Agronomy* **2023**, *13*, 330. [CrossRef]
91. Ahmad, T.; Iqbal, A.; Halim, S.A.; Uddin, J.; Khan, A.; El Deeb, S.; Al-Harrasi, A. Recent Advances in Electrochemical Sensing of Hydrogen Peroxide (H<sub>2</sub>O<sub>2</sub>) Released from Cancer Cells. *Nanomaterials* **2022**, *12*, 73–82. [CrossRef] [PubMed]
92. Talachi, N.; Afzal, E.; Nouri, M.; Abroun, S.; Zarrabi, M.; Jahandar, H. Protective Effect of Human Amniotic Membrane Extract against Hydrogen Peroxide-induced Oxidative Damage in Human Dermal Fibroblasts. *Int. J. Cosmet. Sci.* **2023**, *45*, 73–82. [CrossRef]
93. Hadi, F.; Maqbool, T.; Shakoobi, T.A.; Muhammad, T.; Awan, S.J.; Akhtar, S. Role of Oxidative Stress and Inflammatory Markers in Osteoporosis. *Int. J. Appl. Exp. Biol.* **2022**, *2*, 27–32. [CrossRef]
94. Xing, L.; Zhang, W.; Fu, L.; Lorenzo, J.M.; Hao, Y. Fabrication and Application of Electrochemical Sensor for Analyzing Hydrogen Peroxide in Food System and Biological Samples. *Food Chem.* **2022**, *385*, 132555. [CrossRef]
95. Khan, F.; Shekhar, C.; Mondal, T.; Sabapathy, M. Removal of Industrial Dye and Pharmaceutical Product Using the Nano and Micron-Sized PS Rough Particles Studied with Pt Nanoparticles. *arXiv* **2023**, arXiv:2301.03891.

96. dos Santos Pereira, T.; Mauruto de Oliveira, G.C.; Santos, F.A.; Raymundo-Pereira, P.A.; Oliveira, O.N.; Janegitz, B.C. Use of Zein Microspheres to Anchor Carbon Black and Hemoglobin in Electrochemical Biosensors to Detect Hydrogen Peroxide in Cosmetic Products, Food and Biological Fluids. *Talanta* **2019**, *194*, 737–744. [[CrossRef](#)] [[PubMed](#)]
97. Ciriminna, R.; Albanese, L.; Meneguzzo, F.; Pagliaro, M. Hydrogen Peroxide: A Key Chemical for Today's Sustainable Development. *ChemSusChem* **2016**, *9*, 3374–3381. [[CrossRef](#)] [[PubMed](#)]
98. Sohrabi, H.; Maleki, F.; Khaaki, P.; Kadhom, M.; Kudaiberenov, N.; Khataee, A. Electrochemical-Based Sensing Platforms for Detection of Glucose and H<sub>2</sub>O<sub>2</sub> by Porous Metal–Organic Frameworks: A Review of Status and Prospects. *Biosensors* **2023**, *13*, 347. [[CrossRef](#)] [[PubMed](#)]
99. Maduraiveeran, G. Nanomaterials-Based Portable Electrochemical Sensing and Biosensing Systems for Clinical and Biomedical Applications. *J. Anal. Sci. Technol.* **2022**, *13*, 1–13. [[CrossRef](#)]
100. Dhara, K.; Mahapatra, D.R. Recent Advances in Electrochemical Nonenzymatic Hydrogen Peroxide Sensors Based on Nanomaterials: A Review. *J. Mater. Sci.* **2019**, *54*, 12319–12357. [[CrossRef](#)]
101. Soleymani, M.; Moheb, A.; Babakhani, D. Hydrogen Peroxide Decomposition over Nanosized La<sub>1-X</sub>Ca<sub>X</sub>MnO<sub>3</sub> (0 ≤ X ≤ 0.6) Perovskite Oxides. *Chem. Eng. Technol.* **2011**, *34*, 49–55. [[CrossRef](#)]
102. Navrotsky, A. Thermochemistry of Perovskite-Related Oxides with High Oxidation States: Superconductors, Sensors, Fuel Cell Materials. *Pure Appl. Chem.* **1994**, *66*, 1759–1764. [[CrossRef](#)]
103. Wang, G.; Bao, Y.; Tian, Y.; Xia, J.; Cao, D. Electrocatalytic Activity of Perovskite La<sub>1-X</sub>Sr<sub>X</sub>MnO<sub>3</sub> towards Hydrogen Peroxide Reduction in Alkaline Medium. *J. Power Sources* **2010**, *195*, 6463–6467. [[CrossRef](#)]
104. Dong, W.; Zhao, G.; Song, B.; Xu, G.; Zhou, J.; Han, G. Surfactant-Free Fabrication of CaTiO<sub>3</sub> Butterfly-like Dendrite via a Simple One-Step Hydrothermal Route. *CrystEngComm* **2012**, *14*, 6990–6997. [[CrossRef](#)]
105. Kimijima, T.; Kanie, K.; Nakaya, M.; Muramatsu, A. Hydrothermal Synthesis of Size- and Shape-Controlled CaTiO<sub>3</sub> Fine Particles and Their Photocatalytic Activity. *CrystEngComm* **2014**, *16*, 5591–5597. [[CrossRef](#)]
106. Yang, X.; Fu, J.; Jin, C.; Chen, J.; Liang, C.; Wu, M.; Zhou, W. Formation Mechanism of CaTiO<sub>3</sub> Hollow Crystals with Different Microstructures. *J. Am. Chem. Soc.* **2010**, *132*, 14279–14287. [[CrossRef](#)] [[PubMed](#)]
107. Wang, D.; Guo, Z.; Chen, Y.; Hao, J.; Liu, W. In Situ Hydrothermal Synthesis of Nanolamellate CaTiO<sub>3</sub> with Controllable Structures and Wettability. *Inorg. Chem.* **2007**, *46*, 7707–7709. [[CrossRef](#)]
108. Mahmood, K.; Khalid, A.; Mehran, M.T. MAPbI<sub>3</sub> Microneedle-Arrays for Perovskite Photovoltaic Application. *Nanoscale Adv.* **2019**, *1*, 64–70. [[CrossRef](#)] [[PubMed](#)]
109. Deganello, F.; Liotta, L.F.; Leonardi, S.G.; Neri, G. Electrochemical Properties of Ce-Doped SrFeO<sub>3</sub> Perovskites-Modified Electrodes towards Hydrogen Peroxide Oxidation. *Electrochim. Acta* **2016**, *190*, 939–947. [[CrossRef](#)]
110. He, J.; Zhou, W.; Sunarso, J.; Xu, X.; Zhong, Y.; Shao, Z.; Chen, X.; Zhu, H. 3D Ordered Macroporous SmCoO<sub>3</sub> Perovskite for Highly Active and Selective Hydrogen Peroxide Detection. *Electrochim. Acta* **2018**, *260*, 372–383. [[CrossRef](#)]
111. Wang, X.T.; Li, B.; Kong, D.R.; Zhang, Z.Y.; Zhang, X.F.; Deng, Z.P.; Huo, L.H.; Gao, S. T- and T'-Type Layered Perovskite Ln<sub>2</sub>CuO<sub>4</sub> Nanocrystals for Enhanced Sensing Detection of Hydrogen Peroxide. *J. Alloys Compd.* **2022**, *911*, 165037. [[CrossRef](#)]
112. Qu, X.; Zhao, S.; Gao, P.; Qian, X.; Lu, S.; Duan, F.; Zhu, H.; Du, M. Ultrasensitive Hydrogen Peroxide Electrochemical Sensor Based on Dual-Phase Perovskite Oxide Tubular Nanofiber. *New J. Chem.* **2023**, *47*, 1540–1547. [[CrossRef](#)]
113. Rao, C.N.R. Perovskites. In *Encyclopedia of Physical Science and Technology*, 3rd ed.; Academic Press: Cambridge, MA, USA, 2003; pp. 707–714. ISBN 9780122274107.
114. Hammad, A.B.A.; Magar, H.S.; Mansour, A.M.; Hassan, R.Y.A.; Nahrawy, A.M.E. Construction and Characterization of Nano-Oval BaTi<sub>0.7</sub>Fe<sub>0.3</sub>O<sub>3</sub>@NiFe<sub>2</sub>O<sub>4</sub> Nanocomposites as an Effective Platform for the Determination of H<sub>2</sub>O<sub>2</sub>. *Sci. Rep.* **2023**, *13*, 9048. [[CrossRef](#)]
115. Chakraborty, T.; Das, M.; Lin, C.Y.; Lei, K.F.; Kao, C.H. Highly Sensitive and Selective Electrochemical Detection of Lipocalin 2 by NiO Nanoparticles/Perovskite CeCuO<sub>x</sub> Based Immunosensor to Diagnose Renal Failure. *Anal. Chim. Acta* **2022**, *1205*, 339754. [[CrossRef](#)]
116. Manna, S.; Kumar, S.; Sharma, A.; Sahoo, S.; Dey, M.K.; Mishra, P.K.; Satpati, A.K. RGO/ReO<sub>3</sub> Nano Composite Modified Electrode for the Ultra-Sensitive Determination of Dopamine and Uric Acid. *Biosens. Bioelectron. X* **2022**, *11*, 100156. [[CrossRef](#)]
117. Tamilalagan, E.; Muthumariappan, A.; Chen, T.-W.; Chen, S.-M.; Maheshwaran, S.; Huang, P.-J. A Highly Selective Enzyme-Free Amperometric Detection of Glucose Using Perovskite-Type Lanthanum Cobaltite (LaCoO<sub>3</sub>). *J. Electrochem. Soc.* **2021**, *168*, 086501. [[CrossRef](#)]
118. Boubezari, I.; Zazoua, A.; Bessueille, F.; Errachid, A.; Jaffrezic-Renault, N. Design of a New Non-Enzymatic Sensor Based on a Substituted A<sub>2</sub>BO<sub>4</sub>+δ Perovskite for the Voltammetric Detection of Glucose. *Electroanalysis* **2020**, *32*, 1642–1650. [[CrossRef](#)]
119. El-Ads, E.H.; Galal, A.; Atta, N.F. Electrochemistry of Glucose at Gold Nanoparticles Modified Graphite/SrPdO<sub>3</sub> Electrode-Towards a Novel Non-Enzymatic Glucose Sensor. *J. Electroanal. Chem.* **2015**, *749*, 42–52. [[CrossRef](#)]
120. Xu, D.; Luo, L.; Ding, Y.; Xu, P. Sensitive Electrochemical Detection of Glucose Based on Electrospun La<sub>0.88</sub>Sr<sub>0.12</sub>MnO<sub>3</sub> Nanofibers Modified Electrode. *Anal. Biochem.* **2015**, *489*, 38–43. [[CrossRef](#)] [[PubMed](#)]

**Disclaimer/Publisher's Note:** The statements, opinions and data contained in all publications are solely those of the individual author(s) and contributor(s) and not of MDPI and/or the editor(s). MDPI and/or the editor(s) disclaim responsibility for any injury to people or property resulting from any ideas, methods, instructions or products referred to in the content.